# Cometary globules I. Formation, evolution and morphology

B. Lefloch, Bernard Lazareff

Astron. Astrophys. 289, 559–578 (1994)

ASTRONOMY
AND
ASTROPHYSICS

# Cometary globules

## I. Formation, evolution and morphology

**B. Lefloch**[1] **and B. Lazareff**[2]

[1] Laboratoire d'Astrophysique, Observatoire de Grenoble, Université Joseph Fourier, B.P. 53X, F-38041 Grenoble, France
[2] IRAM, 300 Rue de la Piscine, F-38406 St Martin d'Hères, France

Received 7 January 1994 / Accepted 25 February 1994

**Abstract.** We study the dynamical evolution of a neutral globule illuminated by the ionizing radiation of OB stars. We can reproduce the main morphological and dynamical properties of cometary globules (CGs), which are rather insensitive to initial and boundary conditions. We present results of 2-d hydrodynamical simulations of the evolution of cometary globules. We present a detailed evolutionary sequence from the cloud's collapse to the quasi-stationary cometary regime. This latter phase lasts approximately 90% of the cloud's lifetime. From the results of the simulations, we generate maps of emission measure, projected density and position-velocity diagrams, which can be confronted to optical or molecular line observations. The maps of emission measure exhibit a striking resemblance to various types of CGs and other bright-rimmed structures found in HII regions. A simple analytic model parallels and extends our simulations, including non-thermal pressure support. We derive criteria for the stability of the ionization front in the cometary phase and illustrate them with results from the simulations. We also study the gravitational stability of CGs; we find that they are stable and mainly supported by the magnetic field.

**Key words:** interstellar medium: clouds – interstellar medium: HII regions – interstellar medium: kinematics and dynamics – hydrodynamics

### 1. Introduction

Cometary Globules (CGs) are small isolated clouds (size of a few tenths of a pc) consisting of a dense core prolonged by a long tail, surrounded by a bright rim, and commonly found in the vicinity of OB associations in *HII* regions. In the pioneering work by Reipurth (1983), they have been shown to be active sites of star formation, although usually not gravitationally bound, confirming the conjecture made by Bok (1948) four decades earlier. Early observations revealed that these clouds have simple inner structure and properties (Hawarden & Brand 1976; Zealey et al. 1983). They offer the opportunity of understanding better some of the various mechanisms at work in the large star forming cloud complexes where the situation is much more intricate.

The physical properties as well as the star formation taking place in CGs are strongly dependent on the mechanism of formation and evolution, which is not yet fully established, although recent observations with high angular resolution seem to favour the so-called Radiation-Driven Implosion model (RDI) (see Duvert et al. 1990 for instance). In order to discriminate between the possible models of formation, one needs both a clear evolutionary model for cometary globules from "birth" to "death" and direct observational predictions of this model.

The aim of this article is to present a detailed study of the RDI model in order to answer some of these questions, and fill the present gap between theory and observations.

This model is based on the "rocket effect" introduced by Oort & Spitzer (1955): the UV flux of the OB association ionizes the external layers of the cloud. The ionized gas expands into the interstellar medium. An ionization front preceded by a shock in the neutral gas propagates into the cloud.

The early stages of photoionization of a globule have been numerically simulated by Sandford et al. (1982); they show the collapse of the cloud followed by the formation of a dense core on the cloud's axis; but they did not follow the subsequent evolution of the globule. A first qualitative picture of RDI was proposed by Reipurth (1983) and the first realistic analytical approach was made by Bertoldi (1989) and Bertoldi & McKee (1990). They investigated two major phases in the evolution of the globule: the (early) collapse phase and the stationary cometary regime (when a globule has developed the characteristic head-tail structure). Their results agree with the simulations by Sandford et al. (1982).

Although several points have been established by Bertoldi (1989), Bertoldi & McKee (1990) and Sandford et al. (1982), many questions remain open: what is the evolutionary path of a globule ? Under which condition(s) can it reach the stationary cometary phase and how ? Why are nearly all the observed CGs

*Send offprint requests to*: B. Lefloch

in the cometary phase ? How can we account for the surface corrugations observed, for instance, in many globules of the Gum Nebula ? When and how does star formation occur ? Apart from these questions, we are still lacking *direct observational predictions* which would help to establish (or reject) RDI.

In this article we aim to answer some of these questions and to provide tools for observational diagnostic. We present complete evolutionary sequences, from early ionization until complete dispersal; we derive lifetimes and stability criteria; we suggest qualitative and quantitative observational tests of RDI.

The article is organised as follows: in Sect. 2-3-4 , we describe the hydrodynamical code that we use and the treatment of the coupled equations of radiative transfer and dynamics, the approximations adopted, and the different tests performed on the code; in Sect. 5, we discuss the evolution of globules depending on various initial conditions, and examine the growth of instabilities in the ionization front (Rayleigh-Taylor like) and of gravitational instabilities in the cometary regime. Finally, in Sect. 6, we apply the results from our model to a few cometary globules.

## 2. Physical model

### 2.1. Equation of state

In our numerical simulations, we assume that the gas can exist in three possible states:

1. cold neutral gas having an isothermal sound speed $c_c$ = 0.903 pc My$^{-1}$ (1 pc My$^{-1}$ $\simeq$ 1 km s$^{-1}$), corresponding to $T_n$ = 100 K for atomic H.
2. warm neutral ("intercloud") gas having an isothermal sound speed $c_w$ = 9.03 pc My$^{-1}$, corresponding to $T_w = 10^4$ K
3. ionized gas having an isothermal sound speed $c_i$ = 12.8 pc My$^{-1}$, corresponding to $T_i = 10^4$ K

These values do not attempt to be "exact". The warm neutral phase plays an essentially cosmetic role in allowing an initial state which is in pressure balance. The temperatures are given only for reference, and assuming a pure hydrogen gas; what really matters for the dynamics is the value of the sound speed $c = \sqrt{p/\rho}$. The value of $c_n$ may seem rather large for cold atomic gas, and definitely so for molecular gas; we will return to this point in Sect. 5. We adopt this value only because more "realistic" temperatures of neutral gas would have made the numerical computation more difficult.

The transition from the cold neutral to the warm phase is effected via an equation of state that mimics that of the classical two-phase model:

$$c_n^2 = \begin{cases} c_w^2 & \text{if } \rho \le \rho_c, \\ c_c^2 & \text{if } \rho > \rho_c \end{cases} \quad (1)$$

where $\rho_c$ is 20% of the initial cloud density. The transition from neutral (cold or warm) to ionized gas is effected via the following ansatz that gives c as a function of the ionized fraction $x$:

$$c^{-2} = c_i^{-2} + (c_n^{-2} - c_i^{-2})(1 - \sqrt{x})^2 \quad (2)$$

Generally, $c$ is equal to either $c_n$ or $c_i$ except in the thin transition region of ionization fronts. This formula will be further discussed in Sect. 4.1.

One should note that the sound speed is an explicit function of the density and of the ionized fraction. Physically, this corresponds to the assumption that the timescales for thermal equilibrium are short compared with the dynamical timescales. Computationally, this means that we do not process a differential equation for the energy.

### 2.2. Dynamics

According to the remark above, we have only two dynamical equations. In order to ensure conservation of mass and momentum in the numerical algorithm, we use the corresponding equations in Eulerian form.

$$\frac{\partial \rho}{\partial t} + \nabla \cdot (\rho \mathbf{u}) = 0 \quad (3)$$

$$\frac{\partial \rho \mathbf{u}}{\partial t} + \nabla \cdot (\mathbf{P} + \rho \mathbf{u}\,\mathbf{u}) = 0 \quad (4)$$

which can be rewritten as:

$$\frac{\partial n}{\partial t} + \nabla \cdot (n\mathbf{u}) = 0 \quad (5)$$

$$\frac{\partial n\mathbf{u}}{\partial t} + \nabla \cdot (nc^2\mathbf{I} + n\mathbf{u}\mathbf{u}) = 0 \quad (6)$$

where $\rho$ is the mass density, $n$ the particle (proton) density, $\mathbf{I}$ is the unit rank-2 tensor, and $\mathbf{P} = p\mathbf{I}$ is the isotropic gas pressure. In the second form, all quantities have dimensional equations involving only length and time; this will be used in Sect. 3.

### 2.3. Ionization

In this work, we assume the following values for the ionization cross-section and the recombination coefficient: $\sigma$ = 3 10$^{-18}$ cm$^2$, $\alpha$ = 2.7 10$^{-13}$ cm$^3$ s$^{-1}$ (actually $\alpha_B$, recombination to levels $n \ge 2$). We use the on-the-spot approximation, i.e. we assume that Ly-c photons produced by recombinations are re-absorbed locally. This is marginally justified by the wavelength dependence of $\sigma$, but saves us the considerable complication and numerical load of treating the radiative transfer of recombination photons. The equations for the evolution of the ionized fraction $x$ and the propagation of the Ly-c photon flux $\phi$ along a ray (the line of sight to the illuminating star being in the $z$-direction) can be written:

$$\frac{Dx}{Dt} = -\alpha x^2 n + (1 - x)\sigma\phi(z) \quad (7)$$

$$\frac{d\phi}{dz} = -(1 - x)n\sigma\phi(z) \quad (8)$$

### 2.4. Initial conditions

We take as initial conditions a spherical cloud of uniform density, in the cold neutral state, surrounded by a warm neutral

**Table 1.** Dimensional quantities in cloud photoionization problem

| symbol | parameter | dimens. equation |
|---|---|---|
| $R$ | cloud radius | $L$ |
| $n_0$ | cloud initial H density | $L^{-3}$ |
| $c_n$ | sound speed in neutral gas | $LT^{-1}$ |
| $c_i$ | sound speed in ionized gas | $LT^{-1}$ |
| $\alpha$ | recombination coefficient | $L^3T^{-1}$ |
| $\sigma$ | ionization cross-section | $L^2$ |
| $\Phi$ | Ly-c photon flux | $L^{-2}T^{-1}$ |

intercloud medium in pressure equilibrium. All the gas is initially at rest. While this may not be realistic, it has the merit of introducing a minimum amount of arbitrariness.

The distance $d$ to the illuminating star(s) is assumed to be large compared to the cloud radius. Therefore, we assume the illumination to be plane-parallel, and parameterise it by its Ly-c flux, $\phi$ incident along the $z$ direction.

$$\Phi = \phi(z=0) = N_L/4\pi d^2 \tag{9}$$

where $N_L$ is the total flux of Ly-c photons in photons $s^{-1}$.

## 3. Dimensionless parameters and scalings

Dimensionless parameters constructed from the dimensional problem parameters are a powerful tool to identify major regimes of a physical system. Besides, they allow to generate from one computed solution a whole family of solutions to similar physical problems.

We list in Table 1 the dimensional quantities relevant to our problem. It is apparent that none of the dimensional equations involves mass. This is because, once $c_n$ and $c_i$ have been defined, and using Eq. (2), the dynamical equations (5–6) are in a form that involves only proton density $n$.

The parameters in Table 1 are of two kinds. On one hand, physical constants which we will not vary, that is $c_n$, $c_i$, $\alpha$ and $\sigma$. On the other hand, parameters that allow us to specify various initial and boundary conditions, that is $R$, $n_0$, and $\Phi$. From the latter, one should in principle define three independent dimensionless parameters. We first define an auxiliary parameter, a reference value for the ionized density at the cloud surface. Following previous work on the problem of photoionization of an initially spherical cloud –Oort & Spitzer (1955), Kahn (1969), Dyson (1973), Bertoldi (1989)–, we introduce an effective thickness for the recombination layer, $\eta R$, such that the budget of ionizing photons can be formally written:

$$\Phi = n_i c_i + \eta\alpha n_i^2 R \tag{10}$$

where $\eta$ ($\simeq 0.2$) is a parameter which can be deduced from an analytic solution of the steady-state problem, $n_i$ is the ionized gas density at the cloud surface, and we assume a normal incidence and a D-critical ionization front (hereafter I-front), i.e. the ratio of the ionized to neutral density is $c_n^2/2c_i^2$ and the velocity of the ionized gas, moving away from the I-front, is $c_i$ in the frame of the latter (a classification of ionization fronts and a description of their properties can be found in Osterbrock (1974) and Spitzer (1978)). The nature of the I-front has been shown by Bertoldi (1989) to be approximately D-critical under a wide range of conditions. The budget of ionizing photons shows that $n_i$ depends only on $\Phi$ and the cloud's radius $R$. We actually use Eq. (10) to define a reference value $n_i$, and we will use it instead of $\Phi$ to quantify the intensity of the incident photon flux in the discussion of the parameter space and analytical models. This reference value is distinct from the local, time-dependent $n_i$ determined by the numerical simulations.

We now define the two following dimensionless parameters:

$$\Delta = n_i/n_0 \tag{11}$$

$$\Gamma = \eta\alpha n_i R/c_i \tag{12}$$

The first parameter, $\Delta$, is related to the overpressure of the ionized gas layer with respect to the undisturbed neutral gas:

$$p_i/p_n = 2(c_i/c_n)^2\Delta \tag{13}$$

Note that, since the ionized flow is sonic at the cloud surface, the *total* pressure $p_i + \rho_i u_i^2 = 2p_i$. The second parameter, $\Gamma$, is the ratio of the number of photons used to balance recombinations to those used to bring neutral matter to the ionized state; equivalently, it can be described as the ratio of the outflow timescale $\eta R/c_i$ of ionized gas to its recombination timescale $1/\alpha n_i$.

We now show that the parameter space, which has *a priori* three dimensions ($R$, $n_0$, and $\Phi$ or $n_i$), can be spanned by only two dimensionless parameters $\Delta$ and $\Gamma$, and one simple scaling. Assume we have at hand the solution for a problem defined by values of $R$, $n_0$, and $n_i$, and therefore of $\Delta$ and $\Gamma$. Assume we must solve the problem defined by another set of physical variables $R'$, $n_0'$, and $n_i'$, but having the same two dimensionless variables $\Delta$ and $\Gamma$. Let:

$$k = R'/R \tag{14}$$

Since $\Gamma$ and $\Delta$ have the same value in both problems:

$$n_0' = k^{-1} n_0$$
$$n_i' = k^{-1} n_i$$

and one easily verifies that the following transformation of the solution of the initial problem:

$$\mathbf{r} \longrightarrow k\mathbf{r} \tag{15}$$
$$t \longrightarrow kt \tag{16}$$
$$\mathbf{u} \longrightarrow \mathbf{u} \tag{17}$$
$$n \longrightarrow k^{-1} n \tag{18}$$
$$x \longrightarrow x \tag{19}$$
$$\phi \longrightarrow k^{-1}\phi \tag{20}$$

leaves the equations (5–6, 7–8) invariant.

For a cloud radius $R$, the physical parameters $n_0$, $\Phi$, can be expressed as function of $\Delta$ and $\Gamma$:

$$\Phi = \frac{c_i^2}{\eta\alpha R}\Gamma(1+\Gamma) \tag{21}$$

$$n_0 = \frac{c_i}{\eta\alpha R}\left(\frac{\Gamma}{\Delta}\right) \tag{22}$$

Conversely:

$$\Gamma = \frac{1}{2}\{-1+\sqrt{1+\frac{4\eta\alpha R}{c_i^2}\Phi}\} \tag{23}$$

$$\Delta = \frac{c_i}{2\eta\alpha n_0 R}\{-1+\sqrt{1+\frac{4\eta\alpha R}{c_i^2}\Phi}\} \tag{24}$$

We identify two limiting regimes for the ionizing flux budget:
a) The ionization front, or IF regime, in which the photon flux is consumed mainly in the I-front. This is characterised by $\Gamma \ll 1$
b) The insulating boundary layer, or IBL regime, in which the photon flux is consumed mainly to balance the recombinations in the outflowing gas. This is characterised by $\Gamma \gg 1$.

## 4. Numerical methods

### *4.1. Approximations*

#### 4.1.1. Explicit versus differential energy equation

As mentioned in Sect. 2.1, we use an explicit form $p(\rho, x)$ for the pressure (and internal energy), rather than solve the corresponding differential equation. This is justified by an examination of the thermal timescale:

$$\tau_{cool} = (3kT)/(2n\Lambda(T)) \tag{25}$$

where $\Lambda(T)$ is the cooling function, of the order of $10^{-26}$ erg cm$^3$ s$^{-1}$ for temperatures $T$ of the order of 100K, and small values of the ionized fraction $x$. The ratio of thermal to cloud's dynamical timescale is therefore of the order of:

$$\frac{\tau_{cool}}{\tau_{dyn}} = 7\,10^{-4}\left(\frac{T}{100\ \mathrm{K}}\right)\left(\frac{n}{100\ \mathrm{cm^{-3}}}\right)^{-1}\left(\frac{\Lambda}{10^{-26}\ \mathrm{erg\ cm^3\ s^{-1}}}\right)^{-1} \times\left(\frac{u}{1\ \mathrm{km\ s^{-1}}}\right)\left(\frac{R}{1\ \mathrm{pc}}\right)^{-1} \tag{26}$$

Therefore, for typical values in the cold neutral gas, the approximation of an instantaneous value $p(\rho, x)$ is justified by a comfortable margin.

A similar equation can be written for the thermal and dynamical timescales in the ouflowing ionized gas:

$$\frac{\tau_{cool}}{\tau_{dyn}} = \frac{3kT}{n\Lambda}\frac{u}{\eta R}$$

$$= 0.7\left(\frac{n}{10\ \mathrm{cm^{-3}}}\right)^{-1}\left(\frac{\Lambda}{10^{-24}\ \mathrm{erg\ cm^3\ s^{-1}}}\right)^{-1} \times\left(\frac{u}{10\ \mathrm{km\ s^{-1}}}\right)\left(\frac{R}{1\ \mathrm{pc}}\right)^{-1} \tag{27}$$

$$= 1.1\,\Gamma^{-1} \tag{28}$$

For the ionized gas, the isothermal approximation may fail in the region of parameter space of low values of $\Gamma$; however, this will affect only the dynamics of the outflowing ionized gas, and not the boundary conditions at the ionization front (hereafter I-front) which govern the dynamics of the neutral gas.

#### 4.1.2. I-front transition

The ansatz (2) which we introduced in Sect. 2.1 for the equivalent sound speed in the neutral to ionized transition may seem quite arbitrary, except from the desirable feature that it has the proper limiting values for totally neutral or ionized gas. Our numerical treatment therefore cannot claim to describe the details of the thin transition region from neutral to ionized gas. But all the macroscopic dynamical properties of an ionization front, considered as having a negligible thickness with respect to other flow lengthscales, are contained in the mass and momentum conservation equations, coupled with the ionization budget. Our code is built in order to explicitly conserve mass and momentum. We have exploited the freedom in the choice of the analytic form for (2) to ensure a smooth behaviour of the numerical code in the transition region. We have verified that our code delivers the expected solution for a simple 1-D ionization front problem for which an analytic solution is known (see below in Sect. 4.3).

### *4.2. Algorithms*

We choose a time-explicit Eulerian scheme to study the system of equations (3)–(4)–(7)–(8), and use a grid based on cylindrical coordinates, whose axis of symmetry is the direction of propagation of the incident ionizing flux. We deal with a finite difference equations system that we solve using the "Operator Splitting" (Wilson 1978): in a first Lagrangian step, we solve the ionization equations; in a second Eulerian part, we compute the axial and then radial advective transfers of mass and momentum. We have checked in our numerical tests (see Sect. 4.3) that the degree of asymmetry introduced by this procedure is negligible.

The models presented in this article were generally computed with a 64 (radial) by 192 (axial) grid. For presentation, we symmetrised the maps on a 128 by 192 grid.

The scalar quantities are located at the center of the cells, and the vector quantities at the interfaces. Free boundary conditions are set at the borders of the grid: fictitious cells are set up just outside the boundary with velocities and all the scalar quantities equal to their interior neighbour; the boundary condition has therefore been arbitrarily set to zero gradients. In all cases, the gas which crosses the boundary, be it ionized or neutral, flows supersonically; the choice of the boundary condition therefore

**Table 2.** List of parameters in the simulation

| | |
|---|---|
| $d\phi/dt$ | $1.6\,10^6$ cm$^{-2}$ s$^{-1}$ My$^{-1}$ |
| $\sigma$ | $10^{-19}$ cm$^{-2}$ |
| $\alpha$ | $2.7\,10^{-13}$ cm$^3$ s$^{-1}$ |
| $n_0$ | 10 cm$^{-3}$ |

**Table 3.** Comparison of analytic and numerical results for the plane-parallel photoionization test problem

| | analytic | numerical |
|---|---|---|
| $n_i$( cm$^{-3}$) | 0.756 | 0.748 |
| $n_c$( cm$^{-3}$) | $1.59\,10^2$ | $1.69\,10^2$ |
| $V_c$( pc My$^{-1}$) | 3.56 | 3.43 |
| $V_s$( pc My$^{-1}$) | 3.79 | 3.59 |
| $V_i$( pc My$^{-1}$) | 3.56 | 3.43 |

does not influence the interior flow. The grid can be moved in order to follow the displacement of the main body of the globule.

The equations of ionization (7–8) are solved in two steps: first, $\phi(z+dz)$ is propagated across one cell following Eq. 8:

$$\phi(z+dz) = \phi(z)\cdot\exp(-n\sigma(1-x)dz)$$

Then $x$ can then be deduced from Eq. 7. Since the characteristic ionization time is small compared with the other timescales, we use a first order *implicit* method, that guarantees stability:

$$x(t+dt) = \frac{\sigma\phi + n\alpha x^2(t) + x(t)/dt}{\sigma\phi + 2n\alpha x(t) + 1/dt}$$

The advective transfers are effected using the Piecewise Linear Method (Van Leer 1979). We separately transfer the ionized and neutral fractions of the gas. Strong gradients are stabilised by means of a small amount of viscous pressure. The time step $dt$ is limited by the standard Courant condition (Courant et al. 1967).

### *4.3. Test problems*

#### 4.3.1. Hydrodynamical implosion

We have checked our treatment of the hydrodynamical equations by studying the implosion of an isothermal sphere of cold dense gas (radius $R_0$) surrounded by a hot ambient medium with a strong overpressure: a compression wave propagates into the sphere while a rarefaction wave expands into the hot gas. $P_h$ and $P_c$ being respectively the pressure of the hot and the cold gas, the sphere overshoots an equilibrium state for which the radius is:

$$R_e = R_0(\frac{P_c}{P_h})^{1/3}$$

before bouncing and re-expanding.

We took $n_c = 100\,\mathrm{cm}^{-3}$, $n_h = 10\,\mathrm{cm}^{-3}$, $(P_c/P_h = 20)$ and $R_0 = 0.75$ pc.

Figure 1 shows that spherical symmetry is preserved during the implosion phase down to a minimum radius of 0.22 pc –less than 1/3 of the initial radius– despite the use of a cylindrical coordinate grid. In the ensuing evolution, when the ambient gas slows down the re-expansion, Rayleigh-Taylor instabilities destroy the symmetry.

#### 4.3.2. Steady propagation of an I-front

The treatment of the ionization budget and its coupling to hydrodynamics were tested in the following situation: a box filled with neutral gas of density $n_0$ is uniformly illuminated through one transparent side by an ionizing flux increasing linearly with time. An I-front propagates at a constant speed in the box, and pushes ahead a thin layer of gas compressed through an isothermal shock in the neutral gas, the ionized gas being in quasi-static equilibrium. Let $n_c$ be the density of this layer, $n_i$ the density of the ionized gas, $V_i$ the velocity of the I-front (very close to the velocity $V_c$ of the shocked gas), $V_s$ the velocity of the shock, and let $\Lambda = \alpha^{-1}(d\phi/dt)$. Once the steady regime is reached:

$$\Lambda = n_i^2 V_i$$

$$n_i = \left(\frac{n_0\Lambda^2}{c_i^2}\right)^{1/5} \qquad V_i = \left(\frac{\Lambda c_i^4}{n_0^2}\right)^{1/5} \simeq V_c$$

$$n_c = n_0\left(\frac{\Lambda}{n_i^2 c_n}\right)^2 \qquad V_s = c_n\left(\frac{n_c}{n_0}\right)^{1/2}$$

Table 3 shows that the deviations between numerical and analytical results are at most 6%.

The robustness of the ansatz (2) with respect to the neutral-ionized transition was tested by varying the ratio between the grid size and the photon mean free path.

Different test cases have shown the code to behave satisfactorily for values of $n_0\sigma\delta z$ up to $5\,10^4$, beyond which oscillations develop behind the I-front. Therefore, our code is able to behave reasonably even when the I-front is severely under-resolved.

## 5. Results and discussion

This section is organized as follows. We first discuss the initial properties and gross evolution of clouds in the dimensionless parameter space that was introduced earlier in Sect. 3. Then we concentrate on model 2 ($\Delta = 10^{-1}$ $\Gamma = 10$). We consider separately the collapse phase and the cometary phase: for each of these, we first describe the numerical results, and then derive analytical results and cross-check them with the simulation. We then briefly describe the other three models. The last three subsections are devoted to a discussion of the respective roles of instabilities, magnetic field, and gravity.

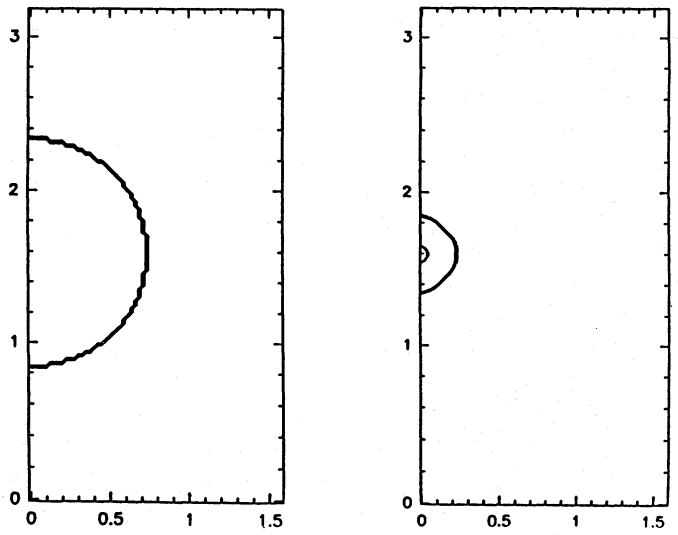


**Fig. 1.** Implosion of an isothermal sphere: Initial configuration and stage near maximum compression at $t = 0.169$ My

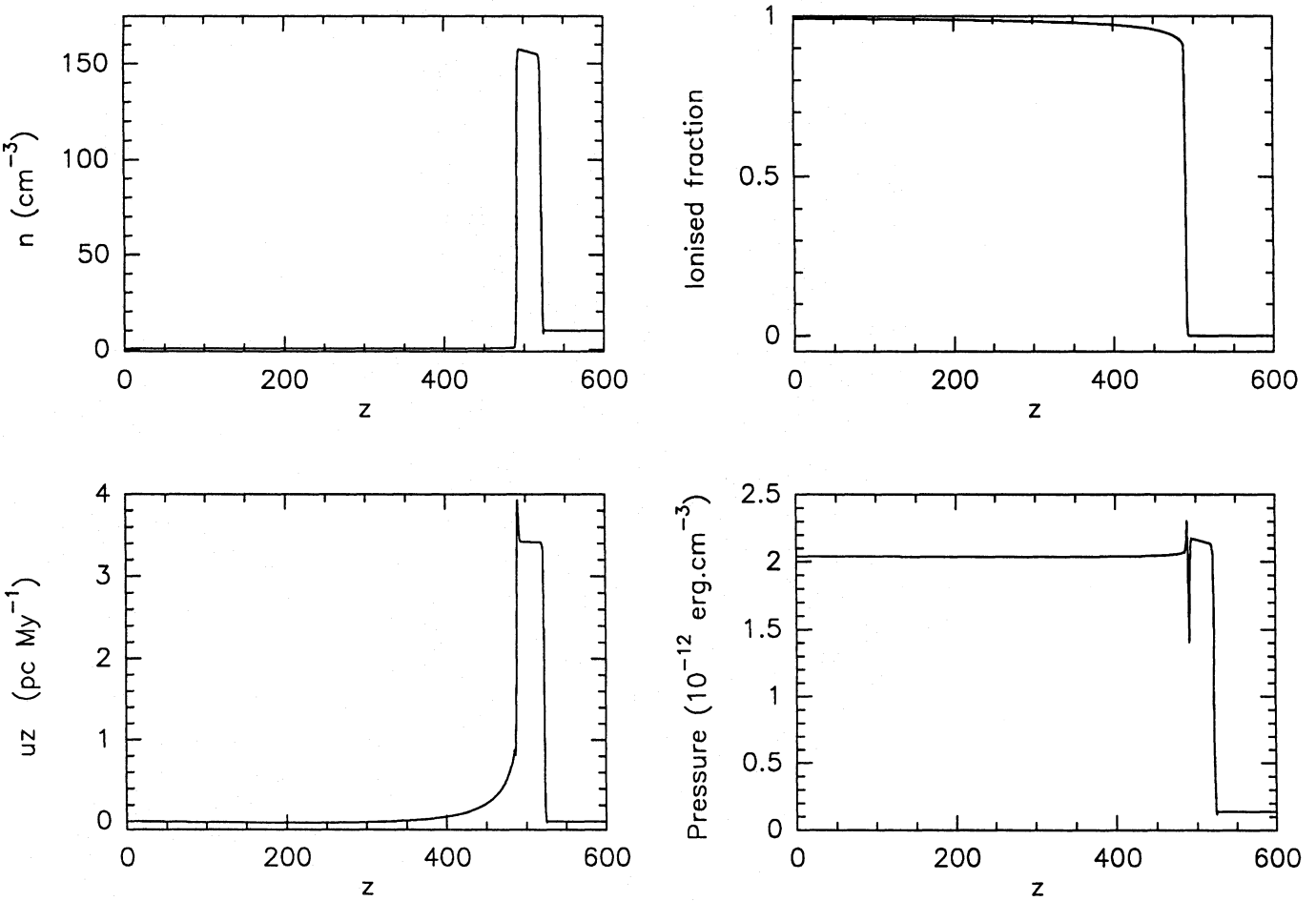


**Fig. 2.** Steady propagation of an ionization front in a box: profiles of density n, ionized fraction x, axial velocity uz and pressure P. One can see from left to right: the ionized region in quasi-hydrostatic equilibrium, the layer of compressed neutral gas, in quasi pressure equilibrium with the ionized gas, and the region of neutral gas at rest

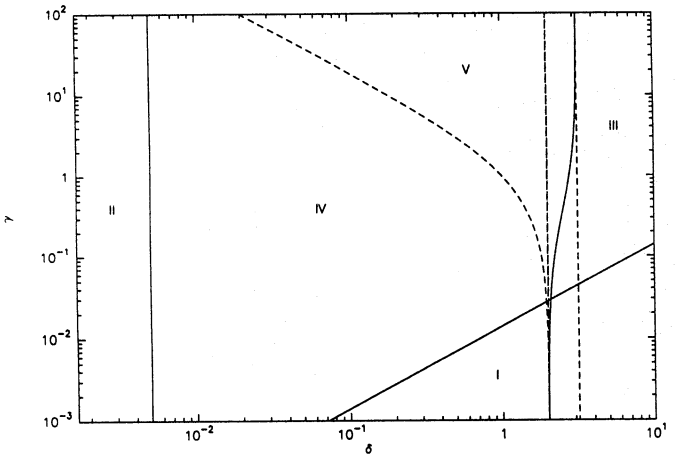


**Fig. 3.** Parameter space: the physically interesting area is limited by solid lines; dashed lines delineate physically different regimes

### 5.1. Parameter space

At least in the first stages of the collapse, the cloud can be described by an effective radius $r(t)$, essentially the radius of the cross-section to the UV photon flux. We generalize Eq. (23)-(24) and define the dimensionless parameters $\delta$ and $\gamma$ relevant to the instantaneous state of the cloud:

$$\gamma(r) = \frac{1}{2}\{-1+\sqrt{1+4\left(\frac{r}{R}\right)\Gamma(1+\Gamma)}\} \qquad (29)$$
$$\gamma(R) = \Gamma$$

$$\delta(r) = \left(\frac{R}{r}\right)\left(\frac{\Delta}{\Gamma}\right)\gamma(r) \qquad (30)$$
$$\delta(R) = \Delta$$

The parameter space is described by the $(\delta-\gamma)$ plane (see Fig. 3). In this plane, the point representative of the state of the cloud moves along the curve $\delta(1+\gamma) = \Phi/n_0 c_i$, towards increasing values of $\delta$ and decreasing values of $\gamma$. This can be understood as follows: as the cloud's radius shrinks, the second term on the right hand side of Eq. (10) decreases, and $n_i$ adjusts itself by an increase, thus increasing the first term on the right hand side, corresponding to an increase of the overpressure $\delta$ and a decrease of the relative contribution $\gamma$ of recombinations to the ionization budget. If and when this evolution brings the cloud from the IBL into the IF regime, there is no further increase in the overpressure, since the ionized gas density at the surface of the cloud is directly determined by the incident flux: $\Phi = n_i c_i$. One should also note that $\delta(r)$ (apart from the factor $2(c_i/c_n)^2$) being the overpressure at the surface of the cloud *relative to the initial state of the cloud*, this parameter is meaningful only during the initial collapse phase, until the shock has crossed the whole cloud.

We first eliminate the region of parameter space where the cloud is initially transparent to Ly-$\alpha$ flux. Let $\tau_0 = n_0 \sigma R$ the initial opacity of the cloud:

$$\tau_0 = \frac{\sigma c_i}{\eta\alpha}\left(\frac{\Gamma}{\Delta}\right) \simeq 71.4\left(\frac{\Gamma}{\Delta}\right) \qquad (31)$$

Therefore, the cloud is transparent to UV photons in the initial stage of its evolution when $(\Gamma/\Delta) \leq 1.4\,10^{-2}$. This defines region $I$.

Outside region $I$ the optical thickness of a cloud to UV photons increases as it is compressed; it will become transparent only when it has almost completely evaporated.

Below $\delta \leq c_n^2/2c_i^2$ is region $II$: the pressure of the ionized gas is too small to compress the gas; there is no noticeable dynamical effect.

In region $III$, the cloud is entirely photo-ionized by an R-weak I-front; the I-front propagates supersonically with respect to the neutral gas at rest: the cloud is permeated by an *ionization flash*. This region is asymptotically limited by the straight lines $\delta = 2$ ($\gamma \ll 1$) and $\delta = \sqrt{10}$ ($\gamma \gg 1$).

In region $IV$, the whole evolution is governed by the propagation of a D-critical I-front preceded by an isothermal shock.

Initial conditions $(\Delta, \Gamma)$ above the limit $\delta(1+\gamma) = 2$, region $V$, result in an I-front of type w-R. It subsequently becomes D-critical due to the growing importance of the recombination layer.

In the following, we concentrate on regions $IV$ and $V$. We have used our numerical code to study the evolution of four models. The global properties of their initial states are listed in Table 4.

Gravity is deliberately not included in our simulations. This point is further discussed in Sect. 5.9.

**Table 4.** Parameters of models studied in numerical simulations

| | $\Delta$ | $\Gamma$ | $n_0$ ($cm^{-3}$) | $\Phi$ ($cm^{-2}\,s^{-1}$) | $R$ (pc) | $M$ ($M_\odot$) |
|---|---|---|---|---|---|---|
| 1 | $10^{-1}$ | $10^{-1}$ | 15.5 | $2.18\,10^6$ | 0.5 | 0.2 |
| 2 | $10^{-1}$ | 10 | 1550 | $2.18\,10^9$ | 0.5 | 20 |
| 3 | 1 | $10^{-1}$ | 1.55 | $2.18\,10^6$ | 0.5 | 0.02 |
| 4 | 1 | 10 | 155 | $2.18\,10^9$ | 0.5 | 2 |

### 5.2. Collapse phase: simulation (model 2)

Figure 4a shows an early stage of the evolution, at $t = 0.036$ My. An isothermal shock progresses into the forward hemisphere of the cloud, leaving behind a thin layer of compressed neutral gas. The ionized gas flows out approximately radially from the ionization front, accelerating into the radial density gradient. The interaction of this outflow with the ambient gas creates two shocks facing away from each other; the inner one is still barely visible in the lower corners of the figure.

At time $t = 0.126$ My a dense core has formed on the axis near the center of the initial cloud (Fig. 4b), while the compressed layer continues to progress into the rear half of the

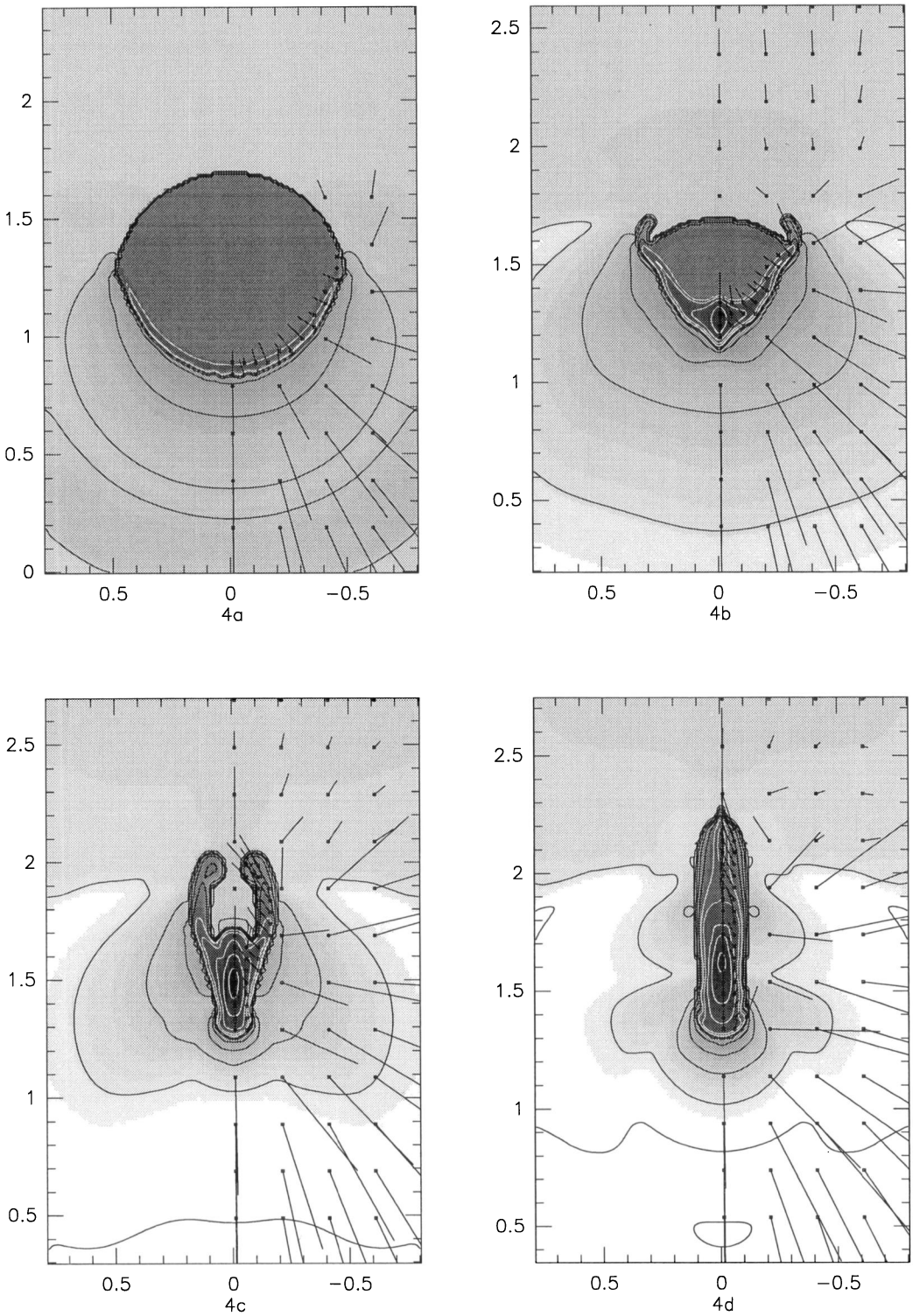


**Fig. 4a–d.** Model 2: Evolution from the early stages of collapse to the maximum compression stage. The ionizing flux shines from the bottom of the page. Snapshots are displayed from left to right and top to bottom: $t = 0.036$ My **a**, 0.126 My **b**, 0.183 My —bf c, 0.210 My **d**. Density contours are spaced by $\Delta \log \rho = 0.5$. Coordinates are in pc. Velocities are represented by vectors of length $u\delta t$, with the scaling time $\delta t = 0.02$ My

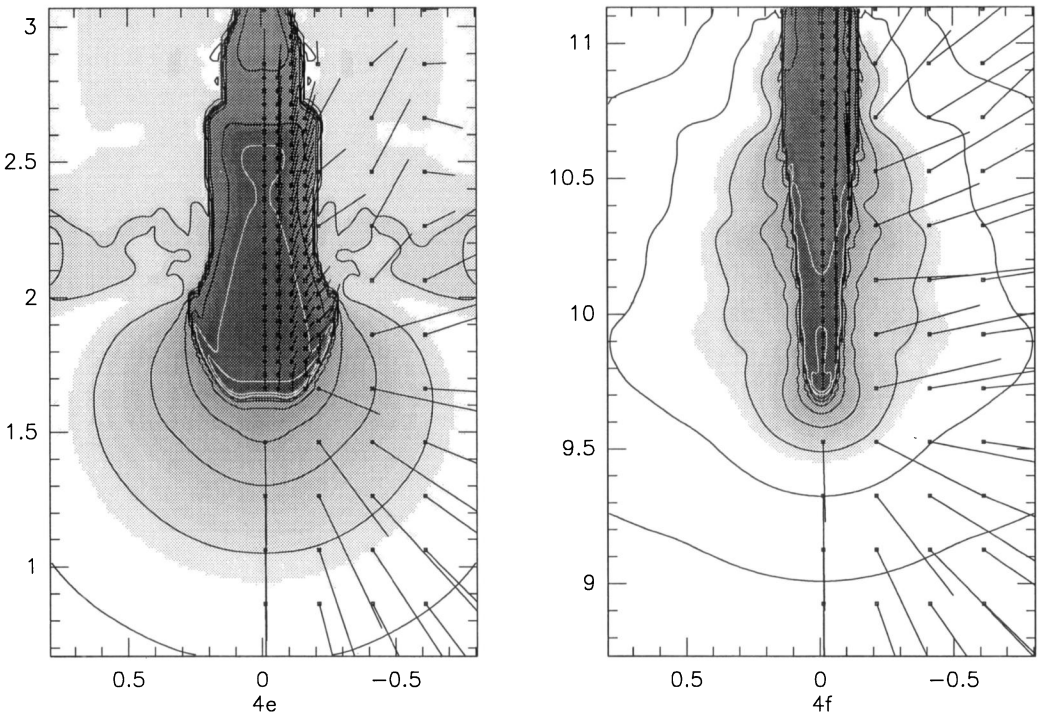


**Fig. 4e–f.** Model 2: Reexpansion stage ($t$ = 0.37 My **e**) and cometary phase ($t$ = 1.30 My **f**)

quiescent cloud. Small "ears" start to develop where the compressed layer meets the rear edge of the initial cloud contour.

At time $t$ = 0.183 My, the compressed layer has almost entirely collapsed onto the axis of symmetry (Fig. 4c), extending the dense core previously mentioned in the direction of positive $z$, while the "ears", now well developed, also converge towards the axis on the rear of the cloud.

The evolution of the cloud's mass versus time is plotted in Fig. 5. During the collapse phase, $\dot{M}_{\rm coll} \simeq 21\ M_\odot\ {\rm My}^{-1}$.

The core is completely formed at $t$ = 0.183 My. Setting a lower limit of $2.0\,10^4$ cm$^{-3}$ for the core density (more than ten times the initial gas density), one finds that most of the mass (80%) is contained within the core (13 $M_\odot$ vs 15.3 $M_\odot$).

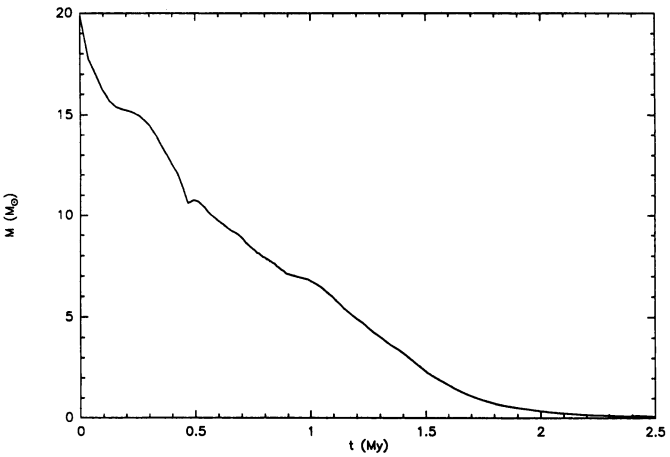


**Fig. 5.** Model 2: Evolution of the cloud's mass vs time. The collapse phase, characterised by a steep mass loss rate, lasts until $t \simeq 0.2$ My. Between 0.2 and 0.45 My, the cloud undergoes its first reexpansion. Afterwards, during the transient phase, the diameter of the cloud remains approximately constant: the mass loss rate and the slope of the curve are constant. There is no clear separation between the transient and the cometary phase which begins at $t \simeq 1.30$ My

### *5.3. Collapse phase: analytical results*

#### 5.3.1. Morphology of collapse phase

Simple considerations allow to explain the main features of the evolution. We return to the early evolutionary stage. The overpressure of the ionized gas drives into the quiescent cloud a layer of compressed neutral gas, which, initially, has a hemispherical shape. The density of ionized gas at the surface point at an angle $\theta$ from the axis (see Fig. 6), is approximately given by:

$$n_i(\theta) = n_i(0)(cos(\theta))^{1/2} \quad (32)$$

$$n_i(0) = (\Phi/\eta\alpha R)^{1/2} \quad (33)$$

These equations are valid for the IBL regime ($\Gamma$ = 10); a cos($\theta$) dependence would prevail in the $\Gamma \ll 1$ case. The compressed layer is driven by the overpressure, and its velocity is approximately given by:

$$u_c(\theta) = u_c(0)(cos(\theta))^{1/4} \quad (34)$$

$$u_c(0) = c_i(2n_i(0)/n_0)^{1/2} = c_i(2\Delta)^{1/2} \quad (35)$$

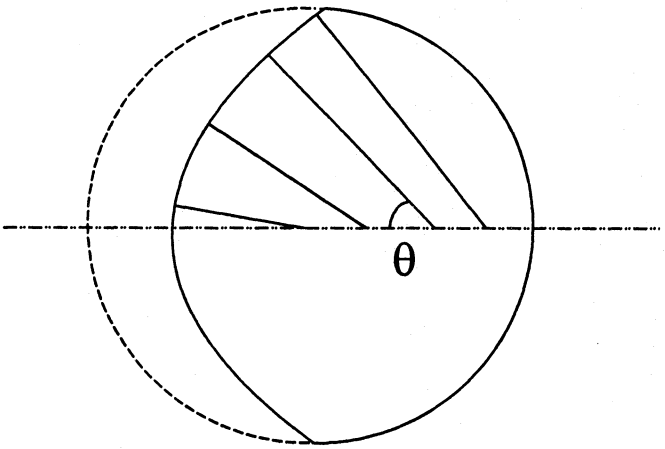


**Fig. 6.** Configuration of the cloud at the beginning of the collapse. The illumination is parallel to the axis; at each point of the surface, it makes an angle $\theta$ with the normal direction. Deviation from spherical symmetry causes normal lines to point farther away on the cloud's axis when $\theta$ increases. The initial (spherical) surface is traced by a dashed contour

In the IF regime, the velocity would vary like $\cos(\theta)^{1/2}$. The velocity of the compressed layer on the axis at $t = 0.036$ My is found to be $u_c = 5.7$ pc My$^{-1}$, in good agreement with the analytical result of Eq. (35): 5.8 pc My$^{-1}$.

The characteristic time for an element of compressed gas to reach the center, $t_{\rm coll} = R/u_c(\theta)$, varies little near the axis. Therefore, a significant fraction of the mass will collapse to a small dense core almost simultaneously, in a time $t_{\rm coll} \simeq 9\,10^{-2}$ My.

Next, note that $t_{\rm coll}$ increases with $\theta$; therefore, the collapse of the peripheral parts of the compressed shell will lag behind that of the central parts. The faster progression of the central parts of the shell with respect to the peripheral parts causes the collapse to deviate from spherical symmetry, and the normal to a surface element points behind the center of the original cloud. As the collapse progresses, further momentum gain (from the ionized gas pressure) is along the normal. Therefore, the peripheral parts of the cloud collapse on the axis, but behind the center of the original cloud, leading to the formation of an elongated dense core. This elongated core is formed in a time which is approximately twice the time of the initial core formation, $t \simeq 2 \cdot t_{\rm coll}$.

For the outermost parts of the cloud ($\theta \simeq \pi/2$), this change of the direction of velocity is so pronounced that their trajectory intersects the rear side of the cloud before collapsing onto the z-axis. When such an element of compressed shell reaches the rear surface of the cloud, the pressure of the ionized gas is no longer balanced by the $\rho u^2$ ram pressure of the quiescent gas (in the frame of the compressed shell), and it is strongly accelerated: this is the origin of the "ears".

#### 5.3.2. Duration and mass loss

During the collapse phase, the mass loss rate and the variation of the mean radius $r$ with time are approximately given by:

$$-\frac{1}{\mu}\dot{M} = 10.4 \left(\frac{\Phi}{10^7\ \mathrm{cm^{-2}\ s^{-1}}}\right)^{1/2} \left(\frac{r}{1\ \mathrm{pc}}\right)^{3/2} M_\odot\ \mathrm{My}^{-1} \quad (36)$$

$$-\frac{dr}{dt} \simeq c_i\sqrt{2\delta} \simeq c_i\sqrt{2\Delta}\left(\frac{R}{r}\right)^{1/4} \quad (37)$$

where $\mu$ is the mean molecular weight.

Taking $< r > \simeq R/2$, we obtain from Eq. (36), $\dot{M}_{\rm coll} \simeq 18\ M_\odot\ \mathrm{My}^{-1}$, close to the 21 $M_\odot$ My$^{-1}$ found in the numerical simulation of the collapse phase.

Similar results for the mass loss and the velocity were obtained in a different form by Bertoldi (1989).

In the IF regime, the previous relations become:

$$-\frac{1}{\mu}\dot{M} = 7.9 \left(\frac{\Phi}{10^7\ \mathrm{cm^{-2}\ s^{-1}}}\right) \left(\frac{r}{1\ \mathrm{pc}}\right)^{2} M_\odot\ \mathrm{My}^{-1} \quad (38)$$

$$-\frac{dr}{dt} \simeq c_i\sqrt{2\Delta} \quad (39)$$

We take $1/\sqrt{2\Delta}(R/c_i)$ as estimate of the collapse time; the mass evaporated during the core formation is therefore:

$$\frac{\Delta M}{M} \equiv 1 - f \quad (40)$$

$$= \frac{2}{11}\sqrt{2\Delta} \quad (41)$$

In the IF regime, the corresponding expression is:

$$\frac{\Delta M}{M} = \frac{1}{8}\sqrt{2\Delta} \quad (42)$$

Our analysis shows that the main properties of the cloud in the collapse are determined by $\Delta$ and are quite insensitive to $(c_i/c_n)$, therefore to the temperature of the cold neutral gas. This is because during the collapse phase, the dynamics of the cold gas are dominated by ram pressure ($\rho u^2$) terms.

### *5.4. Cometary phase: simulation (model 2)*

When the compressed gas first converges to the axis, the cloud overshoots the compression corresponding to the equilibrium state: Figure 4d ($t = 0.210$ My) shows the state of maximum compression. Figure 4e ($t = 0.37$ My) shows the cloud near maximum re-expansion. Re-compression occurs through the formation of a compressed layer pushed by the ionized gas, like in the initial collapse phase. The cloud also gains further axial momentum through this process. It then undergoes a series of radial oscillations with decreasing amplitude. Figure 7 shows the evolution with time of "radial momentum" defined as $1/2\pi \int \rho_n u_r d^3v$

In this transient phase ($t = 0.6 - 1$ My), the maximum radial dimension of the globule remains approximately constant: $r = 0.2$ pc; the mass of the globule decreases *roughly* linearly with

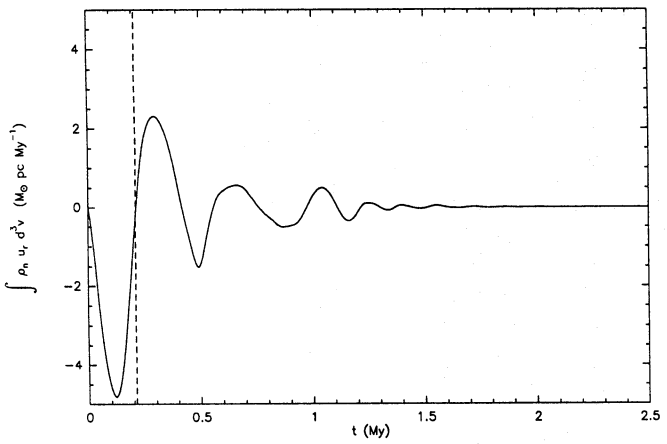


**Fig. 7.** Model 2: Evolution of the cloud's "radial momentum" vs time. The amplitude of oscillations decreases with time and is negligible in the cometary phase ($t \geq 1.30$ My)

time and $\dot{M} = 9\ M_\odot\ \mathrm{My}^{-1}$ (see Fig. 5), while Eq. (36) provides an estimate of $\dot{M} = 13\ M_\odot\ \mathrm{My}^{-1}$.

At $t = 1.30$ My (Fig. 4f) the cloud, now cometary shaped, has nearly reached a quasi-equilibrium state. The mass is now $4.0 M_\odot$ and $f = 0.22$.

As the cloud evaporates and accelerates away, its radius decreases. Ultimately, the cloud is entirely ionized for $t \geq 2.7$ My.

### *5.5. Cometary phase: analytical results*

In the cometary phase the cloud tends to a quasi-equilibrium state, in which a cometary head is confined by the pressure of the ionized gas and shields the comet tail from the photon flux.

That quasi-equilibrium state satisfies the following conditions:

a) the cloud structure is stationary in an accelerated frame

b) the gas follows an hydrostatic stratification

c) the gas density and the incident photon flux allow a direct transition at every surface point from the interior medium to the ionized gas through a critical-D ionization front without an intervening shock-compressed layer.

A simple argument allows to derive an approximate analytic expression for the radius $R_e$ of the cometary head in the quasi-equilibrium phase. Qualitatively, the decrease in the interior pressure due to hydrostatic stratification as one moves away from the head is balanced by the obliquity of the illumination by UV photons. An exact calculation of the cloud shape can be found in Bertoldi & McKee (1990). An approximate value for $R_e$ can be found as follows. A point on the surface located $R_e$ away from the cloud head in the axial direction sees an I-front pressure an order of magnitude smaller than at the head, because of the obliquity of the photon flux. In order to satisfy condition c) above, there must be a matching decrease in the interior pressure. The latter one varies over the hydrostatic lengthscale $H = c_n^2/g$, where $g \simeq 2\pi\rho_i c_i^2 R_e^2/M_e$ is the acceleration received from the ionized gas. Therefore:

$$R_e \simeq H \tag{43}$$

Hence we infer the implicit relation between $R_e$ and $\gamma(R_e)$

$$R_e = \left(\frac{fM}{2\pi m_H}\right)\left(\frac{c_n}{c_i}\right)\left(\frac{\eta\alpha}{c_i}\right)^{1/2}\gamma^{-1/2} \tag{44}$$

In contrast to the discussion of Sect. 3, the cloud's radius is no longer a free parameter, but is determined by Eq. (44). Therefore, the parameter space has one less dimension. In dimensional variables, this corresponds to the fact that, for fixed $\Phi$, all clouds having the same mass reach the same equilibrium radius, independent of their initial radius. The only remaining dimensionless parameter is $\gamma$.

In the IBL regime, and for molecular gas of standard composition (mean molecular weight $\mu = 2.36$), different from the pure atomic hydrogen assumed in the numerical simulations, we obtain from Eq.(44):

$$\left(\frac{R_e}{1\ \mathrm{pc}}\right) = 0.078\left(\frac{M_e}{M_\odot}\right)^{2/5}\left(\frac{\Phi}{10^7\ \mathrm{cm^{-2}\ s^{-1}}}\right)^{-1/5} \times \left(\frac{T_n}{100K}\right)^{2/5} \tag{45}$$

We can also derive the following:

$$\left(\frac{R_e}{R}\right) = \left(\frac{2f}{3}\right)^{2/5}\left(\frac{c_n}{c_i}\right)^{4/5}\Delta^{-2/5} \tag{46}$$

which shows, not surprisingly, that the ratio $R_e/R$ is only a function of the initial compression ratio $2(c_i/c_n)^2\Delta$. From Fig. 4, we get $R_e \simeq 0.065$ pc, in agreement with Eq. (46) which predicts $R_e = 0.070$ pc.

In the IF regime, we have the similar relations:

$$\left(\frac{R_e}{R}\right) = \left(\frac{2f}{3}\right)^{1/3}\left(\frac{c_n}{c_i}\right)^{2/3}\Delta^{-1/3} \tag{47}$$

$$\left(\frac{R_e}{1\ \mathrm{pc}}\right) = 0.113\left(\frac{M_e}{M_\odot}\right)^{1/3}\left(\frac{\Phi}{10^7\ \mathrm{cm^{-2}\ s^{-1}}}\right)^{-1/3} \times \left(\frac{T_n}{100K}\right)^{1/3} \tag{48}$$

Using Eq.(41-36), we can estimate the lifetime $t_{\mathrm{com}}$ of the globule in the cometary phase:

$$t_{\mathrm{com}} = fM/|\dot{M}(R_e)|$$

$$t_{\mathrm{com}} = 1.28\left(\frac{R}{c_i}\right)\left(\frac{c_i}{c_n}\right)^{6/5}\Delta^{-2/5}\left(1 - \frac{2}{11}\sqrt{2\Delta}\right)^{2/5} \tag{49}$$

which in the present case gives $t_{\mathrm{com}} \simeq 3$ My, in good agreement with our simulations.

$$\left(\frac{t_{\mathrm{com}}}{1\ \mathrm{My}}\right) = 3.6\left(\frac{M_e}{M_\odot}\right)^{2/5}\left(\frac{\Phi}{10^7\ \mathrm{cm^{-2}\ s^{-1}}}\right)^{-1/5} \times \left(\frac{T_n}{100K}\right)^{-3/5} \tag{50}$$

In the IF regime, the previous relations become:

$$t_{\rm com} = 1.75 \left(\frac{R}{c_i}\right)\left(\frac{c_i}{c_n}\right)^{4/3} \Delta^{-1/3}\left(1-\frac{1}{8}\sqrt{2\Delta}\right)^{1/3} \quad (51)$$

$$\left(\frac{t_{\rm com}}{1\,{\rm My}}\right) = 6.5\left(\frac{M_{\rm e}}{M_\odot}\right)^{1/3}\left(\frac{\Phi}{10^7\,{\rm cm^{-2}\,s^{-1}}}\right)^{-1/3} \times\left(\frac{T_{\rm n}}{100K}\right)^{-2/3} \quad (52)$$

Simulations show that a succession of phases of compression and re-expansion persists during a transition period whose duration is $t_{trans} \simeq 10\, t_{\rm coll}$.

The ratio of the transient to the cometary phase lifetimes results, in the IBL regime, as:

$$\frac{t_{\rm trans}}{t_{\rm com}} = 5.5\left(\frac{c_i}{c_n}\right)^{-6/5}\Delta^{-1/10}\left(1-\frac{2}{11}\sqrt{2\Delta}\right)^{-2/5} \simeq 0.23\left(\frac{T_{\rm n}}{100K}\right)^{3/5}\Delta^{-1/10} \quad (53)$$

using the weak dependence of $t_{\rm com}/t_{\rm coll}$ on $f$.

In the IF regime:

$$\frac{t_{\rm trans}}{t_{\rm com}} = 4.0\left(\frac{c_i}{c_n}\right)^{-4/3}\Delta^{-1/6}\left(1-\frac{1}{8}\sqrt{2\Delta}\right)^{-1/3} \simeq 0.12\left(\frac{T_{\rm n}}{100K}\right)^{2/3}\Delta^{-1/6} \quad (54)$$

The lifetime of the cometary phase depends only weakly on $\Delta$, and so does the ratio $t_{\rm trans}/t_{\rm com}$. Given the values of this ratio, both in the IBL and the IF regime, one concludes that *although it appears unlikely to observe a globule in the initial collapse phase, there is a non-negligible chance to observe a globule in the transient phase with the characteristic kinematical signature of shock waves* (see below Sect. 6.3).

In contrast with the collapse phase, the properties of the cloud during the cometary phase *do* depend on the actual value of $c_{\rm n}$. The value adopted for $c_{\rm n}$ in the numerical simulations implies that they underestimate the lifetime in the cometary phase. This remark does not affect our analytical estimates.

Besides, in a realistic situation, gravity, star formation, and time variations of the UV flux will affect the globule's evolution.

### *5.6. Other models*

#### 5.6.1. Model 4: $\Delta = 1$ $\Gamma = 10$

At the beginning of the collapse phase, the ionized gas behind the ionization front moves towards the cloud, that is characteristic of a R-weak I-front. Progressively, the I-front slows down and becomes D-critical. The subsequent evolution is similar to the one of case 2.

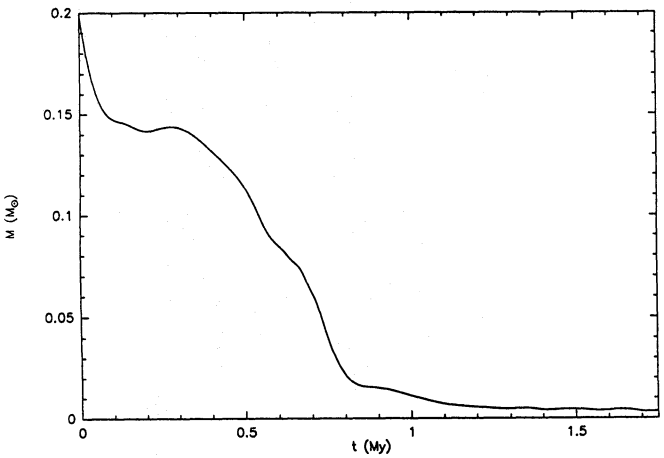


**Fig. 8.** Model 1: Evolution of the cloud's mass vs time. This curve shows the 3 phases in globule's evolution: collapse ($t \leq 0.2$ My), transient, and cometary phase ($t \geq 0.9$ My). Most of the mass has been evaporated in the transient phase because of instabilities in the I-front

#### 5.6.2. Model 1: $\Delta = 10^{-1}$ $\Gamma = 10^{-1}$

This model, (like model 3 below) is remarkable mainly by the occurrence of instabilities in the I-front. These instabilities appear at the head of the globule, after the collapse phase. They result in a marked enhancement of the mass loss rate between 0.3 My and 0.8 My (see Fig. 9). A small fraction of the initial mass survives as a quasi-stationary cometary globule. The instabilities are analysed in Sect. 5.7.

#### 5.6.3. Model 3: $\Delta = 1$ $\Gamma = 10^{-1}$

The global evolution of the cloud is similar to and even more drastic than in case 1. The mass loss due to the instabilities is too large to enable the cloud to reach a quasi-equilibrium state. It ends completely ionized.

### *5.7. Instabilities*

To analyse the stability of the globule in the cometary, quasi-stationary regime, we consider separately scales which are either small or large with respect to the effective thickness $\eta R$ of the ionized gas layer.

#### 5.7.1. Small scales

Capriotti (1973) analysed the stability of a plane-parallel D-critical I-front with a gravity (real or apparent) in the front rest frame. In his analysis, for the unperturbed state, the ionized gas density is uniform. The conditions of Capriotti's analysis are approximately met when the perturbation wavelength satisfies: $\lambda \ll \eta R < R$. Capriotti showed that the condition for small-scale perturbations of a D-critical I-front to be unstable is:

$$g\,\tau_{\rm rec} > 2\frac{n_i}{n_c}c_i \quad (55)$$

where $n_c$ is the density of the neutral gas ahead of the I-front. Using:

$$g \simeq \frac{1}{M} 2\pi \rho_i c_i^2 r^2$$
$$M \simeq \frac{4\pi}{3} \rho_c r^3$$
$$\tau_{\rm rec} \simeq 1/\alpha n_i$$

the criterion of Capriotti can be reformulated as:

$$\frac{\alpha n_i r}{c_i} \lesssim 1 \quad (56)$$
$$\gamma \lesssim 1 \quad (57)$$

For a cloud in the cometary stage, the previous condition is achieved for:

$$\log\left(\frac{M_e}{M_\odot}\right) \lesssim 2.42 - 2\log\left(\frac{\Phi}{10^7 \text{ cm}^{-2}\text{ s}^{-1}}\right) - \log\left(\frac{T_n}{100K}\right) \quad (58)$$

Therefore, in the IF regime, the small-scale perturbations are unstable. This can be understood from a simple physical argument. When recombinations are negligible, the flux incident on the front is not perturbed. Therefore, the static and dynamic pressure terms on the downstream side of the I-front are constant, and so is the (dominant) static pressure of the neutral gas at the I-front boundary. Under the presence of gravity $g$, this is just the condition for simple Rayleigh-Taylor instability.

#### 5.7.2. Large-scale perturbations

When the wavelength $\lambda$ of the perturbation is larger than $\eta R$, one of the working hypotheses of Capriotti's analysis breaks down. We propose below an approximate analysis for scales $\lambda$ which are in the range $\eta R < \lambda \lesssim R$. Admittedly, since $\eta \approx 0.2$, our analysis is only approximate for a restricted range.

In the regime $\gamma < 1$, as explained above, we have again a simple Rayleigh-Taylor instability: all scales are unstable.

In the recombination-dominated regime, $\gamma > 1$, the properties of the I-front and its associated ionized gas layer adjust *locally* to deformations of the cloud surface, in particular to the pressure in the neutral gas just inside the I-front. This can be described by an effective surface tension $\Pi$, following Chièze & Lazareff (1980):

$$\Pi = \frac{1}{2} \frac{\partial P_c}{\partial(1/r)} \quad (59)$$

where $P_c$ is the pressure of the neutral gas. The effective surface tension in the recombination-dominated regime can be expressed as:

$$\Pi = \frac{1}{2} \rho_i c_i^2 r \quad (60)$$

These approximations enable us to apply the analysis of the Rayleigh-Taylor instability (Chandrasekhar 1961). The smallest unstable wavelength results as:

$$\lambda_{\rm min} \simeq \frac{2\pi}{\sqrt{3}} r \quad (61)$$

This rough analysis shows that the smallest unstable wavelength is of the order of $2r$.

The results of our analysis are summarised as follows:
When recombinations are not dominant, $\gamma < 1$, all scales are unstable during the cometary phase.
When recombinations are dominant, only scales comparable to the cloud diameter are unstable.
This is illustrated in Fig. 9 by the morphology of two globules in the cometary phase, having respective values $\gamma = 10^{-2}$, and $\gamma = 2$, when instabilities start to grow.

### 5.8. *Influence of a non-thermal pressure*

In most astrophysical situations, a *non-thermal* pressure, of turbulent or magnetic origin, contributes to support molecular clouds against collapse, the kinetic pressure being by far insufficient.

We argue in Sect. 6 below that magnetic pressure is the dominant support mechanism. A rigorous treatment of the effects of the magnetic field requires complex calculations, generally with numerical methods. Bertoldi (1989) gives approximate analytic results for simple configurations of a large-scale magnetic field.

Here we assume the magnetic field to be tangled on small scales, and we restrict our discussion to the cometary phase, which we have shown in Sect. 5.5 to be the most likely to be observed.

In order to take into account this non-thermal pressure we define the ratio $\beta$ of the non-thermal to thermal pressure: $P_{\rm nt} = \beta P_{\rm kin}$. If the cloud is supported by a magnetic field, we obtain for constant $\beta$ the empirical law of Heiles $B^2/\rho = 8\pi\beta c_n^2$. The hydrostatic lengthscale in the globule becomes: $H = (1+\beta)c_n^2/g$.

Both the equilibrium radius and the lifetime of the cometary globule are modified:
in the IBL regime

$$R_{\rm nt} = R_e \cdot (1+\beta)^{2/5} \quad (62)$$
$$t_{\rm nt} = t_{\rm com} \cdot (1+\beta)^{-3/5} \quad (63)$$

in the IF regime:

$$R_{\rm nt} = R_e \cdot (1+\beta)^{1/3} \quad (64)$$
$$t_{\rm nt} = t_{\rm com} \cdot (1+\beta)^{-2/3} \quad (65)$$

The magnetic pressure increases the value of the cometary radius, as a consequence of an extra support against the pressure of the ionized gas. As the mass loss rate depends only on the incident flux $\Phi$ and on the illuminated surface of the cloud, $\dot{M}$ increases and the lifetime of the cometary globule decreases.

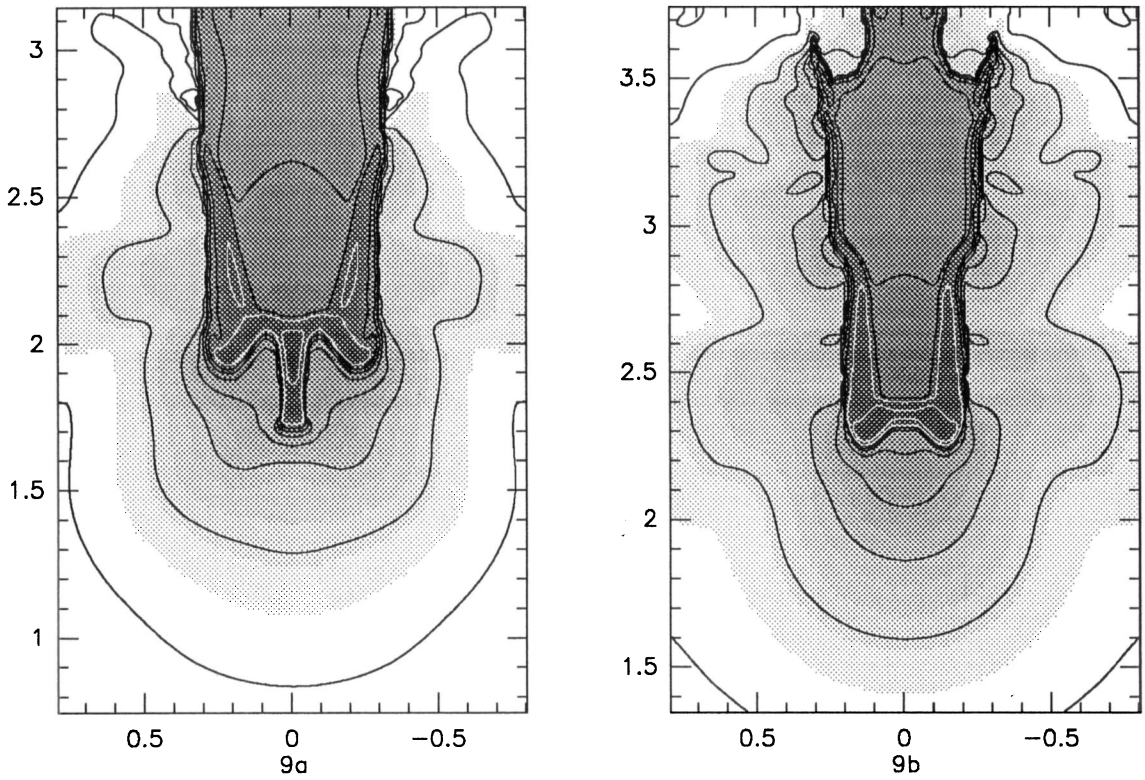


**Fig. 9. a** Small scale instabilities in the cometary phase at $t$ = 0.57 My in model 1. $\gamma \simeq 5.10^{-3} - 10^{-2}$ when the instability begins to grow. Small wavelength modes also develop near the axis. **b** Large scale instabilities in the cometary phase at $t$ = 0.47 My in model 2. $\gamma \simeq 2$ when the instability begins to grow. The dominant mode corresponds to $\lambda \simeq 2r$

*5.9. Gravity*

For all the cases we have studied, gravity appears negligible, and was deliberately ignored. In Sect. 3, we showed that any photoionization problem is fully characterised by the knowledge of the two dimensionless parameters ($\Delta$, $\Gamma$) and the cloud's radius R; this one determines the importance of gravitation. Thus, to each set ($\Delta$, $\Gamma$) correspond two classes of clouds, according to whether they are self-gravitating or not. In the latter case, their evolution can be properly described by our code.

However, the fact that IRAS sources and bipolar outflows in CG's are very often found at the edge of clouds strongly suggests that gravity can play an active role even in the early stages of evolution. The next step to describe better the evolution of a photo-ionized globule is to incorporate gravitation in our code.

Nevertheless, the results of our modelling enable us to study the gravitational stability of globules in the cometary phase, which is the necessary condition to detect globules at this stage: stability results from the balance between thermal pressure (and eventually magnetic pressure) on one side, and gravity and ionization on the other side.

We first consider the case of a thermally supported cloud.

The cloud is stable if its mass is lower than the Ebert-Bonnor mass associated to the globule, that is:

$$M_e \lesssim M_{BE} \simeq 1.18\, c_n^4 \cdot \left(G^3 P_e\right)^{-1/2} \qquad (66)$$

where $P_e$ is the external pressure at the surface of the cloud, $P_e \simeq 2\rho_i c_i^2$.

Using Eq.(45)–(48) the condition for gravitational stability is, respectively in the IBL and in the IF regime:

$$\log(\frac{M_e}{M_\odot}) \leq 1.69 - \frac{1}{3}\log(\frac{\Phi}{10^7\ \mathrm{cm^{-2}\ s^{-1}}}) + \frac{7}{3}\log(\frac{T_n}{100K}) \qquad (67)$$

$$\log(\frac{M_e}{M_\odot}) \leq 1.77 - \frac{1}{2}\log(\frac{\Phi}{10^7\ \mathrm{cm^{-2}\ s^{-1}}}) + 2\log(\frac{T_n}{100K}) \qquad (68)$$

The transition between the two ionization regimes is given by:

$$\log(\frac{M_e}{M_\odot}) = 2.42 - 2\log(\frac{\Phi}{10^7\ \mathrm{cm^{-2}\ s^{-1}}}) + \log(\frac{T_n}{100K}) \qquad (69)$$

For a magnetically supported cloud ($\beta \gg 1$), the criterion of gravitational stability is given by: $M \leq 0.12\, G^{-1/2} F$ (Spitzer 1978), where $F \simeq \pi B R_e^2$ is the magnetic flux threading the

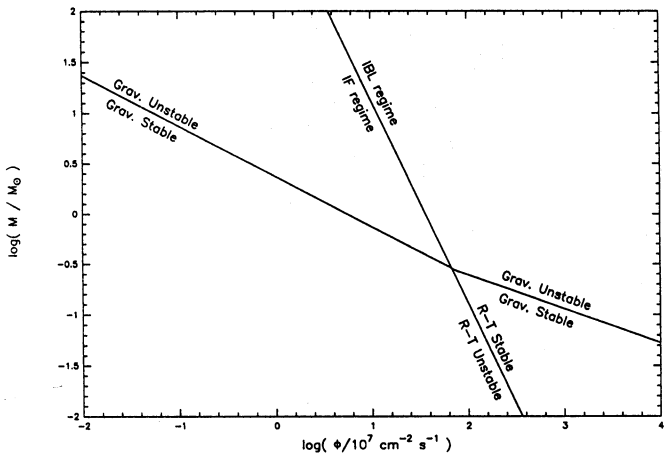


**Fig. 10.** Stability of a thermal cometary globule: the limits are drawn for molecular hydrogen at a kinetic temperature of 20 K

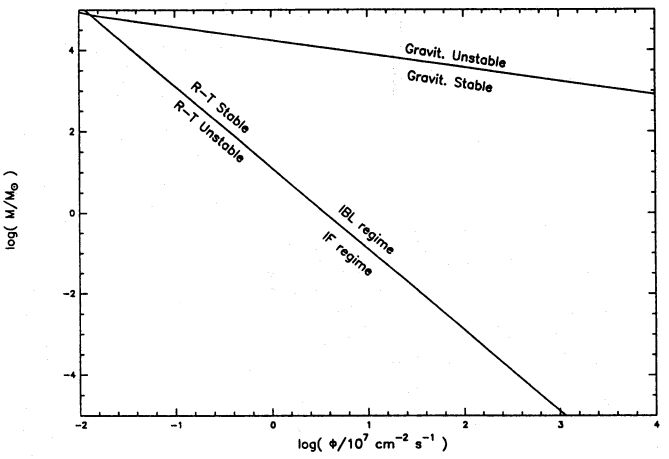


**Fig. 11.** Stability of a magnetized cometary globule: we assume molecular hydrogen at a kinetic temperature of 20 K and $\beta = 100$. All magnetized cometary globules are Rayleigh-Taylor unstable in the IF regime. More remarkable is the fact that the critical mass for gravitational collapse is larger than $10^3\ M_\odot$ for "realistic" values of the ionization flux, so that any magnetized globule is gravitationally stable

cloud. Expressing the magnetic field B as a function of $\beta$, the condition reads respectively for the IBL and the IF regime:

$$\log(\frac{M_e}{M_\odot}) \leq 1.21 - \frac{1}{3}\log(\frac{\Phi}{10^7\ \mathrm{cm^{-2}\ s^{-1}}}) + \frac{7}{3}\log(\frac{\beta T_n}{100K}) \quad (70)$$

$$\log(\frac{M_e}{M_\odot}) \leq 1.34 - \frac{1}{2}\log(\frac{\Phi}{10^7\ \mathrm{cm^{-2}\ s^{-1}}}) + 2\log(\frac{\beta T_n}{100K}) \quad (71)$$

The boundary between the two regimes is modified in the following way:

$$\log(\frac{M_e}{M_\odot}) = 2.42 - 2\log(\frac{\Phi}{10^7\ \mathrm{cm^{-2}\ s^{-1}}}) + \log(\frac{\beta T_n}{100K}) \quad (72)$$

Figure 11 summarizes the criteria for hydrodynamical and gravitational instabilities. We have assumed $T = 20$ K, appropriate for molecular gas in the vicinity of OB stars and $\beta = 100$, anticipating on a typical value which we derive in Sect.6 for observed cometary globules.

Two conclusions can be drawn:
First, globules whose ionization budget is dominated by photons in the I-Front are Rayleigh-Taylor unstable.
Second, cometary globules with masses of at most a few $M_\odot$ are stable against gravitational collapse.

### *5.10. Modified initial and boundary conditions*

Globules with a bright rim often appear as small-scale deformations ($\approx$ 1 pc) of the boundary of a large (tens of pc) $H^+$ region; they are not isolated, and, in particular, the ionized gas cannot expand freely laterally, but is constrained by the large-scale, roughly plane-parallel, flow.

We have performed a calculation where the radial boundary of the computational volume had a $v_r = 0$ boundary condition, mimicking the conditions described above and where the initial gas condensation is modelled as a core surrounded by a less dense envelope. The resulting morphology, a blunt-nosed cone having an opening angle of $\approx 90^o$, similar to a barnacle, is rather common in Sharpless regions.

These bright rimmed globules which are not Cometary Globules, as defined by Leung (Leung 1985), are very likely formed by RDI and differ only by their morphology from true CGs.

## 6. Comparison with observations

### *6.1. Optical morphology*

The optical morphology of cometary globules is dominated by the emission of recombination lines. We have computed surface brightness maps by integrating along each line of sight $n_e^2\ dl$. These maps are computed for an inclination of $30^o$. Since the gross properties of our models are relatively insensitive to our two dimensionless parameters $\Gamma$ and $\Delta$, we have only one parameter, the age, to match the model with observations. Figure 12 shows a comparison of selected object images (POSS red plates) with model brightness maps.

Frame a (bottom left) shows an anonymous CG near the center of the $H^+$ region S190: The axis of the CG is oriented towards the ionizing flux source (O-B stars 6 pc away in the NW direction); the cloud is surrounded by an approximately circular envelope of expanding ionized gas which reconnects to the ambient medium through a shock. Frame b (top left) shows a stage in the evolution of the ($\Delta = 0.1, \Gamma = 10$) model, at time $t = 0.135$ My, in the dynamical compression phase.

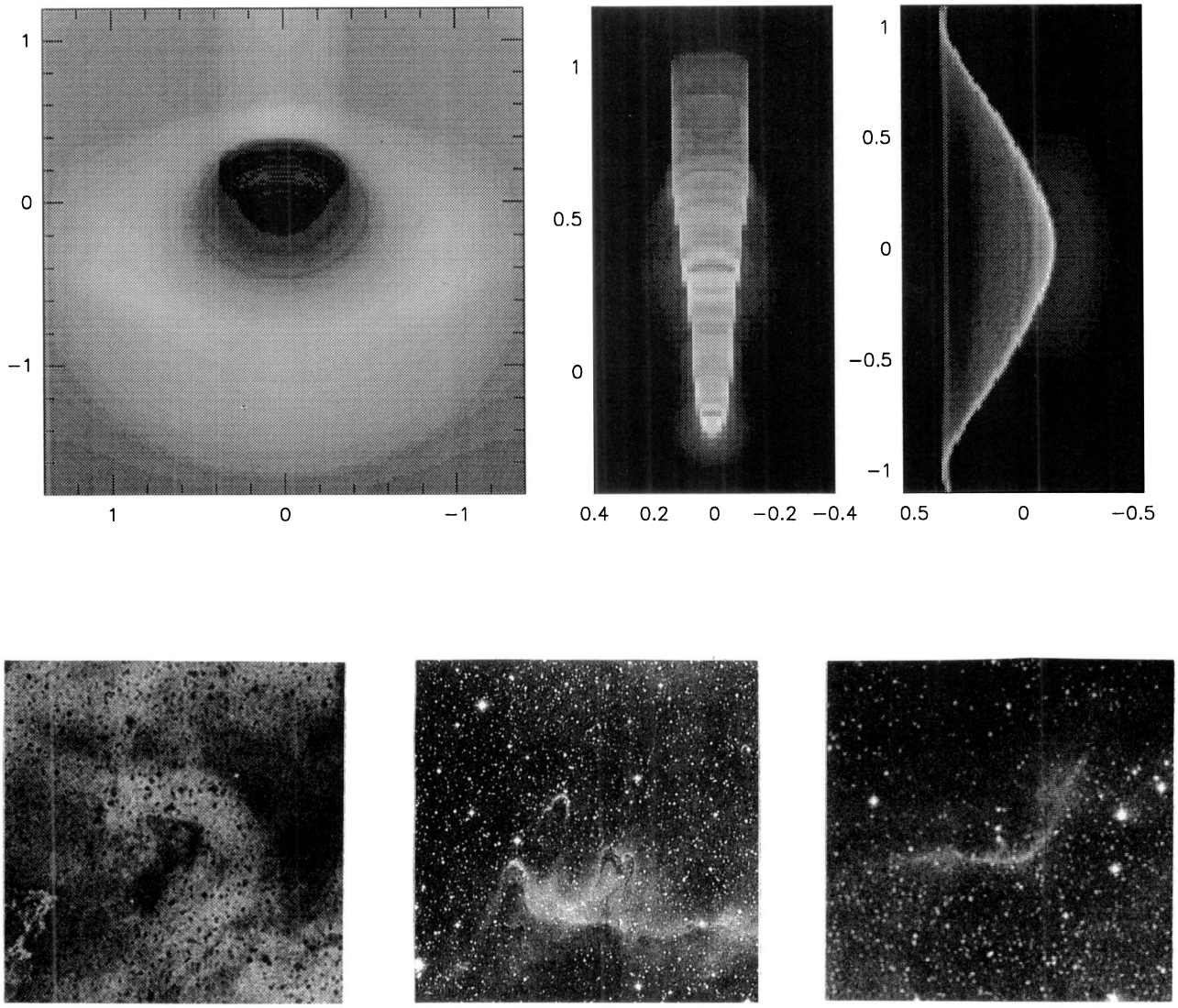


**Fig. 12.** Comparison between the optical morphology and the brightness map of 3 typical globules: on the upper panel are shown the computed emissivity maps of globules, respectively in the collapse and the cometary phase, and an example of simulated bright rim. The linear dimensions are in pc. On the lower panel are reproduced 3 POSS of CGs from the atlas of Neckel & Vehrenberg (1985)

Frame a (bottom center) shows a few cometary globules of the H*II* region S199, illuminated on their right by an O star (not visible on the picture). Frame b (top center) shows a simulated globule in the cometary stage, at time $t = 1.30$ My.

Frame a (bottom right) shows a globule with a bright rim at the border of the $H^+$ region S199, close to CG13 in the catalogue by Sugitani et al. (1991). Frame b (top right) shows a globule simulated with the modified initial and boundary conditions described in Sect.5.10, which lies in the plane of the sky.

In all three cases, the agreement between simulations and optical observations is extremely encouraging.

### 6.2. *Quantitative analysis of observed globules*

We have applied our model to 4 globules present in physically very different regions: GN 21.38.9 (Duvert et al. 1990), TDR10 and TDR13, two tear drops of the Rosette Nebula (González-Alfonso & Cernicharo 1993) and CG6, a globule of the Gum Nebula (González-Alfonso et al. 1993). Their kinematics shows no evidence for collapse or large-scale motion, so that we can reasonably assume *these globules to be in a stage close to the cometary equilibrium.*

#### 6.2.1. Observational data

GN 21.38.9 is illuminated by an O6 type star, 12 pc away from the globule. We estimate its Ly-c luminosity from Panagia (1973) as $N_{\rm L} = 10^{49}\ {\rm s}^{-1}$. The ionizing flux impinging on GN 21.38.9 is therefore $\Phi \approx 5.8\,10^8\ {\rm cm}^{-2}\ {\rm s}^{-1}$, ignoring possible projection effects.

The Rosette nebula is excited by 5 O type stars, whose spectral types range from O9 to O4, and a B0 star. Following Dorland (1986), we take $N_{\rm L} = 8.5\,10^{49}\ {\rm s}^{-1}$. TDR10 and TDR13 are 10 pc away from the ionizing stars, so that the ionizing flux is estimated as: $\Phi = 7.1\,10^9\ {\rm cm}^{-2}\ {\rm s}^{-1}$.

Estimating $\Phi$ is more difficult in the case of the Gum Nebula, as already discussed by Reipurth (1983); we adopt his value $N_{\rm L} = 8.5\,10^{49}\ {\rm s}^{-1}$. CG6 is approximately 50 pc away from the ionizing sources, so that it is exposed to a flux $\Phi = 2.9\,10^8\ {\rm cm}^{-2}\ {\rm s}^{-1}$.

The other observational data are taken from the articles cited above for each of the globules, and are summarised in table 5.

#### 6.2.2. Analysis and results

We first determine the ionization regime by comparing the ionizing flux $\Phi$ to the critical flux $\Phi_{\rm c}$ for which $\Gamma = 1$ (this condition is similar to Eq.(72)):

$$\Phi_{\rm c} = \frac{2c_{\rm i}^2}{\alpha\eta R} \tag{73}$$

For all of these four globules, the main part of the incident ionizing flux is consumed in recombinations in the IBL.

We infer the ionized gas density at the cloud's surface, hence the ionized gas pressure (assuming $T_{\rm i} = 10^4$ K).

$$P_{\rm i} = 4.22 \cdot \left(\frac{\Phi}{\alpha\eta R_{\rm core}}\right)^{1/2} \cdot k_{\rm B} T_{\rm i} \tag{74}$$

From the FWHM $< \Delta v >$, we compute the non-thermal velocity component $\sigma_{\rm NT}$ of the gas, and the inner turbulent pressure. Both the turbulent pressure $P_{\rm turb}$ and kinetic pressure $P_{\rm kin}$ are evaluated from the mean $H_2$ density $n$: $n = 3M_{\rm core}/4\pi\mu R_{\rm core}^3$.

The last column of Table 6 gives for each of the four globules the ratio $\omega$ of gravitational energy to the virial surface term $3P_{\rm i}V$. It appears that gravity plays a negligible role in these cometary globules as already mentioned in Sect. 5.9. Yet GN 21.38.9 contains an embedded outflow, and numerous other CGs of similar properties contain embedded IRAS sources (Sugitani et al. 1991). Therefore such embedded protostellar sources must have formed in an earlier phase of the evolution. Maybe the transient compression encountered in the collapse phase enhances ambipolar diffusion and triggers gravitational collapse.

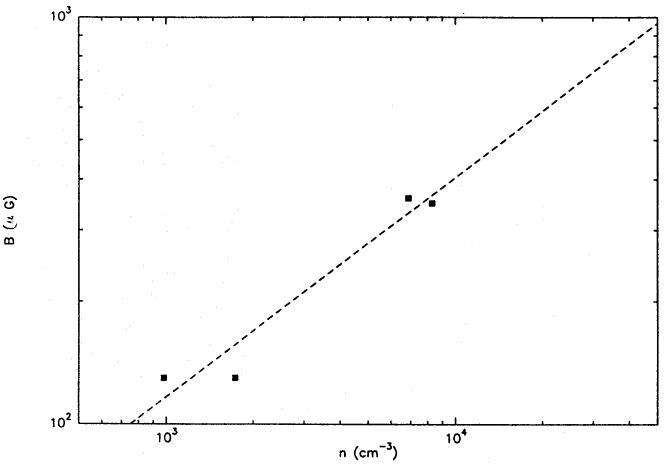


**Fig. 13.** Variation of B vs n for the 4 studied globules. Superimposed is the least square fit: $B = 2.8n^{0.54}$ (dashed line)

Since gravity plays a negligible role, these globules are bounded by the pressure of the outflowing ionized gas. However, *neither the thermal pressure nor the turbulent pressure can support the clouds against the outer pressure*: these quiescent cometary globules appear to be supported against collapse predominantly by the magnetic field pressure.

The strength of the magnetic field is estimated by equating the cloud's total inner pressure (thermal plus turbulent plus magnetic) to the ionized gas pressure. The value we infer for the magnetic pressure allows us to compute the lifetime of the globules $t_{\rm com}$ by Eq.65; $t_{\rm com}$ is actually a lower limit since we make use of the core mass and not of the whole mass. In Table 6 we summarise the results of our study, in particular the value of the magnetic field we infer and the lifetime of these globules.

In Fig. 13 we plot the magnetic field's strength versus the particle density that we derive for all of these globules. A least square fit shows that $B \simeq 2.8\,n^{0.54}$: *the magnetic field seems to follow the Heiles' law* empirically obtained for self-gravitating clouds (Heiles 1993).

The main conclusions which come out of our analysis are:
a) *these isolated globules are mainly supported by magnetic field ($B \approx 10^2\mu$G) and not by turbulence*, unlike what is usually observed in molecular clouds where there is rough equipartition between magnetic and turbulent pressures. (Myers & Goodman 1988).
b) gravity plays a negligible role in their present state, and the presence of embedded stellar objects is a puzzle.

### 6.3. *Velocity structure*

We have computed velocity-position maps for a typical globule at different times of the main stages of evolution, for an optically thin molecular transition. The parameters of the globule

**Table 5.** Observational characteristics of the globules

| | $\Phi$ ($10^7$ cm$^{-2}$ s$^{-1}$) | $M_{core}$ ($M_\odot$) | $R_{core}$ (pc) | $\Delta v_{FWHM}$ (km s$^{-1}$) | $T_K$ (K) |
|---|---|---|---|---|---|
| GN 21.38.9 | 58 | 4 | 0.24 | 1.8 | 30 |
| CG6 | 29 | 1 | 0.125 | 1.0 | 15 |
| TDR10 | 710 | 0.48 | 0.058 | 0.94 | 20 |
| TDR13 | 710 | 0.32 | 0.054 | 0.71 | 20 |

**Table 6.** Results inferred from the model

| | $P_i$ (erg cm$^{-3}$) | $P_{kin}$ (erg cm$^{-3}$) | $P_{turb}$ (erg cm$^{-3}$) | $< B >$ ($\mu$G) | $\beta$ | $t_{com}$ (My) | $\omega$ |
|---|---|---|---|---|---|---|---|
| GN 21.38.9 | $7.0\,10^{-10}$ | $5.0\,10^{-12}$ | $2.7\,10^{-11}$ | 130 | 142 | 0.3 | $1.2\,10^{-3}$ |
| CG6 | $5.2\,10^{-10}$ | $4.4\,10^{-12}$ | $1.5\,10^{-11}$ | 130 | 157 | 0.3 | $1.3\,10^{-3}$ |
| TDR10 | $5.0\,10^{-9}$ | $2.8\,10^{-11}$ | $6.1\,10^{-11}$ | 350 | 176 | 0.09 | $5.0\,10^{-2}$ |
| TDR13 | $5.2\,10^{-9}$ | $2.3\,10^{-11}$ | $2.8\,10^{-11}$ | 360 | 220 | 0.06 | $2.2\,10^{-2}$ |

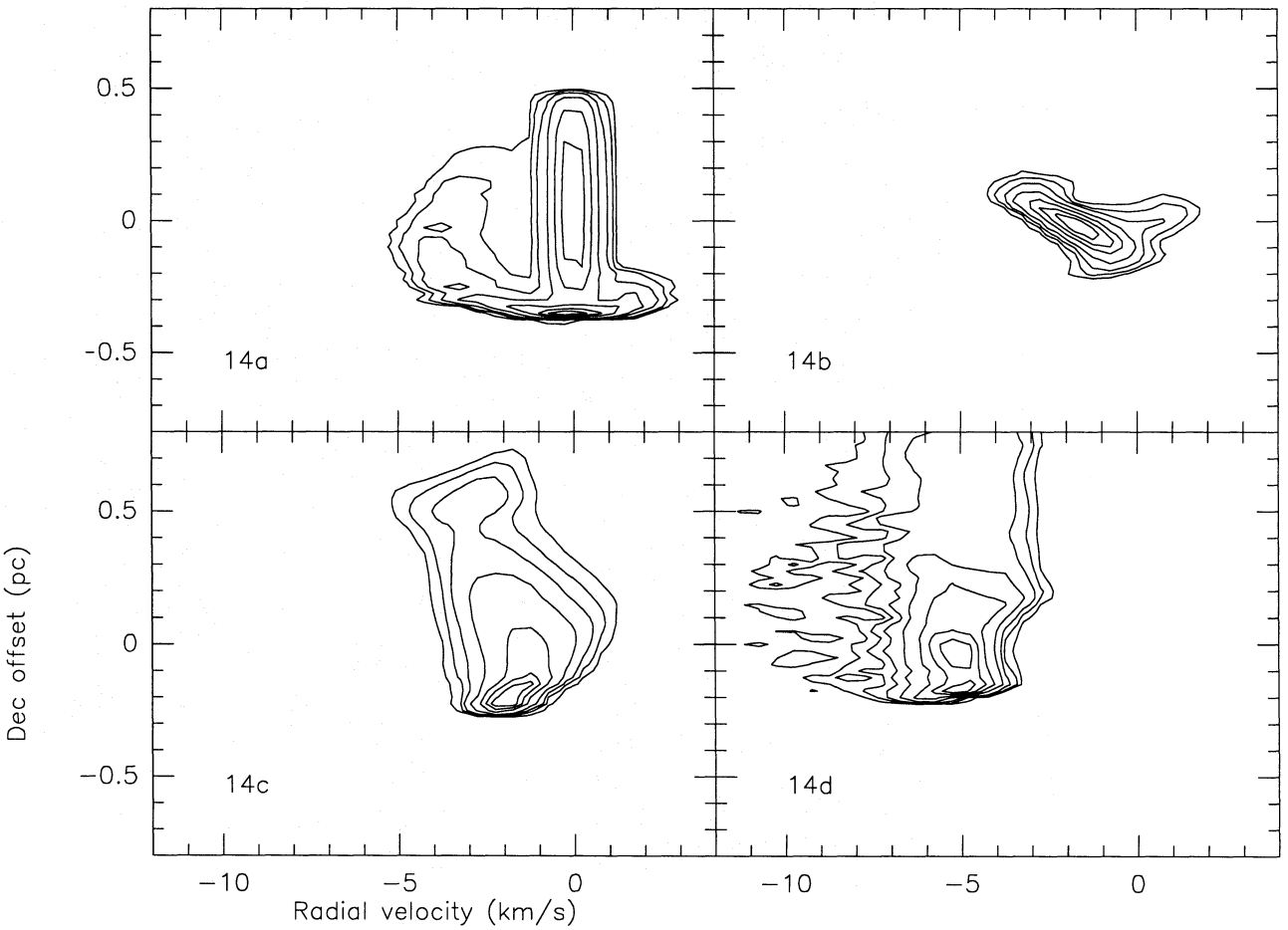


**Fig. 14.** Velocity-position cut along the axis of the globule for different stages of model 2 at times $t = 0.036$ (collapse), $t = 0.183$ (near maximum compression), $t = 0.328$ (reexpansion), $t = 1.30$ My (cometary phase); the related density-velocity maps are shown in Fig. 4

were taken from model 2 and the cloud is assumed to have an inclination angle of 30° with respect to the plane of the sky. The results we derive are not very sensitive to the set of parameters chosen.

In the early collapse ($t$ = 0.036 My, see Fig. 4a), two wings trace the signature of the shocked gas (Fig. 14a):
a) a prominent blue wing associated to the compressed gas moving towards the observer (the rear side gas).
b) a small red wing revealing the compressed gas moving away from the observer (on the front side).

At the end of the collapse phase, when the cloud is turning into an elongated dense core ($t$ = 0.183, see Fig 4c), the gas is accelerated through the tail while the rear sides of the cloud are collapsing on the axis. This acceleration and the rear side gas are responsible for the (strong) "blue" velocity gradient. ($\approx 10\,\mathrm{km\,s^{-1}\,pc^{-1}}$, see Fig. 14b). The red wing located behind the head of the globule is emitted by the front side gas.

Figure 14c shows the velocity-position diagram when the cloud is reexpanding ($t$ = 0.37 My, see Fig. 4d): the overall blue velocity gradient is caused by the acceleration of the gas across the tail. A "red" velocity gradient originates from the head; this is because the compressed gas in the head moves faster than the gas immediately behind it. A large red wing, $\approx 3\,\mathrm{km\,s^{-1}}$ wide, located behind the head, corresponds to the reexpanding rear side gas.

In the cometary regime, ($t$ = 1.30 My, Fig. 14d), only a very weak overall velocity gradient remains. Numerous small clumps ejected and accelerated along the globule appear in the diagram as "fuzz" on the blue side.

As a conclusion, only the pre-cometary phase has a non-ambiguous spectroscopic signature, characterised by an overall blue velocity gradient and the presence of wings emitted by gas located behind the head, which moves towards or away from the cloud's axis, depending on its degree of evolution. The only remarkable feature associated with the cometary phase is the presence of small blue "residuals" tracing some material ejected and flowing along the globule.

Patel et al. (1993) have observed a globule in the Rosette Nebula which exhibits the characteristic double kinematic component of the pre-cometary phase. However, photoionization alone can not account for the velocity shift (approximately $10\,\mathrm{km\,s^{-1}}$) between the two emission components. Numerous globules in the cometary phase have been observed and a weak radial velocity gradient is often present (Duvert 1990; González-Alfonso et al. 1993). These observations will be analysed in more detail in a forthcoming article devoted to observational tests of the kinematic signature of RDI (Lefloch & Lazareff 1994).

## 7. Conclusion

In this work, we have studied the evolution of a globule illuminated by a planar Ly-c photon flux: the mechanism of radiatively driven implosion (RDI) leads to the formation of the so-called "Cometary Globules". The evolution of a cloud is controlled by two dimensionless parameters: the ratio $\Delta$ of the ionized gas to the initial cloud's densities, and the fraction $\Gamma$ of UV photons absorbed in the IBL.

For a wide range of values of these parameters, including those found in typical H*II* regions, RDI is a two-stage process:
a) collapse phase: it occurs over a short time-scale (typically $10^5$ yr). Maximum compression, possibly leading to star formation, occurs in the early stages of the collapse. After maximum compression, the globule undergoes a few expansions and re-compressions. This pre-cometary phase lasts $\simeq$ 10% of the cloud's lifetime. This stage is spectroscopically characterized by a double component or possibly more complex emission line profile.
b) cometary phase: the globule is in a quasi-hydrostatic equilibrium. There is no remarkable spectroscopic signature. The lifetime of this stage is of the order of a few $10^5$ yr to a few My. Some globules in fact never experience such a relatively long cometary phase. If the photon budget is dominated by the I-front (as opposed to the recombinations), small-scale instabilities develop at the end of the collapse phase and cause a rapid dispersal and destruction of the cloud.

This mechanism applies not only to the isolated globules, located in the interior of H*II* regions, but also to the "barnacle shaped" globules observed at the boundary of these regions.

Our model reproduces the optical morphology of cometary globules:
- invoking only one physical mechanism: photoionization.
- using only one free parameter, the degree of evolution; the results are relatively insensitive to the two other parameters, $\Delta$ and $\Gamma$.

Other observational tests of the model concerning the kinematic signature of the collapse phase will be presented in a forthcoming article (Lefloch & Lazareff 1994).

Because cometary globules are relatively simple, isolated objects, they lend themselves to a rather detailed comparison between observations and modelling. In particular, our model allows us to determine the strength of the magnetic field inside globules, which seems to follows Heiles' empirical law (1993).

This detailed comparison can shed light on the mechanisms of support against gravity and star formation in these clouds. In particular, one may ask if the predominance of the magnetic energy density over the turbulent energy density observed in our (very) limited sample of globules reveals a more general trend in CGs and perhaps in small size clouds ?

*Acknowledgements.* We thank Dr. S. Cabrit and Dr. T. Forveille for their careful and critical reading of an early version of the manuscript which greatly helped to improve this work.

## References

Bertoldi, F.,1989, ApJ, 346, 735
Bertoldi, F.,McKee, C., 1990, ApJ, 354, 529
Bok, B.J., 1948, Centennial Symposia, Harvard Obs. Monograph no 7, 53
Brandt, P.W.J.L., Hawarden, T.G., Longmore, A.J., Williams, P.M., Caldwell, J.A.R., 1983, MNRAS, 203, 215

Capriotti, E.R., 1973, ApJ, 179, 495
Dyson, J.E., 1973, A&A, 27, 459
Cernicharo, J., Bachiller, R., Gonzalez-Alfonso, E., Gómez-González, J., 1992, A&A, 261, 589
Chandrasekhar, S., 1961, Hydrodynamic and Hydromagnetic Stability, (Oxford Univ. Press)
Chièze, J.P., Lazareff, B., 1980, A&A, 91, 290
Dorland, H., Montmerle, T., Doom, C., 1986, A&A, 160, 1
Duvert, G., Cernicharo, J., Bachiller, R., Gómez-González, J., 1990, A&A, 233, 190
Giulani, J.L., 1979, ApJ, 233, 280
Gonzalez-Alfonso, E., Cernicharo, J., 1993, ApJ Letters (submitted)
Gonzalez-Alfonso, E., Cernicharo, J., Radford, S., 1993, A&A, (submitted)
Hawarden, T.G., Brandt, P.W.J.L., 1976, MNRAS, 175, 19p
Heiles, C., Goodman, A., McKee, C., Zweibel, E., 1993, in Protostars and Planets III, ed. E.H. Levy & J.J. Lunine, (Tucson & London: Univ. of Arizona Press)
Kahn, F.D., 1969, Physica, 41, 172
Lefloch, B., Lazareff, B., 1994, in prep.
Leung, C.M., 1985, in Protostars & Planets II, ed. D. Black & M. Matthews (Tucson: Univ. of Arizona Press).
Myers, P.C., Goodman, A.A., 1988, ApJ, 329, 392
Neckel, T., Vehrenberg, H., 1985, Atlas of Galactic Nebulae, Treugesell-Verlag K.G. D-4000 Düsseldorf
Oort, J.H., Spitzer, L.Jr, 1955, ApJ, 121, 6
Osterbrock, D., E., 1974, Astrophysics of Gaseous Nebulae, ed. G. Burbidge, W.H. Freeman and Company (San Francisco).
Panagia, N., 1973, As.J, 78, 929
Patel, N.A., Xie, T., Goldsmith, P.F., 1993, ApJ, 413, 593
Reipurth, B., 1983, A&A, 117, 183
Sanford, M.T., Whitaker, R.W., Klein, R.I., 1982, ApJ, 260, 183
Spitzer, L.Jr, 1978, Physical processes in the Interstellar Medium, J. Wiley & sons (New York).
Sugitani, K., Fukui, Y., Ogura, K., 1991, ApJ Supp., 77, 59
Van Leer, B., J. Comp. Phys, 1979, 32, 101
Woodward, P.R., 1976, ApJ, 207, 484
Zealey, W.J., Ninkov, Z., Rice, E., Hartley, M., Tritton, S.B., Ap Letters, 1983, 23, 119

This article was processed by the author using Springer-Verlag LaTeX A&A style file version 3.